

# Instability of hypersonic flow over a cone

By SHARON O. SEDDOUGUI<sup>1</sup>†  
AND ANDREW P. BASSOM<sup>2</sup>

<sup>1</sup>School of Mathematics, University of New South Wales, Sydney 2052, Australia

<sup>2</sup>Department of Mathematics, University of Exeter, North Park Road, Exeter,  
Devon, EX4 4QE, UK

(Received 21 November 1995 and in revised form 15 May 1997)

The linear stability analysis of hypersonic flow over a sharp slender cone with an attached shock is described. Attention is focused on the viscous modes of instability which may be described by a triple-deck structure. The situation in which both the effect of the shock and the influence of curvature are important is considered in the weak-interaction region. Both neutral and non-neutral solutions are presented for both axisymmetric and non-axisymmetric disturbances. The results obtained suggest that the effect of curvature on the stability of hypersonic flow is significant when the attached shock is taken into account.

---

## 1. Introduction

The recent interest in developing high-speed aircraft has increased the need to understand hypersonic flow and in particular the effect of shocks. Significant progress has been made in the study of hydrodynamic stability of boundary layers at hypersonic speeds. Smith (1989) showed that the stability of such a boundary layer to viscous modes may be described by a triple-deck structure and within this framework Cowley & Hall (1990, hereafter referred to as CH), considered the effect of an attached shock on the stability of the hypersonic flow over a wedge. They showed that the shock can have a significant effect on the growth rates of Tollmien–Schlichting waves and, crucially, the presence of the shock was found to allow an infinite number of unstable modes: a situation which is unable to arise in the absence of the shock.

Concurrent with CH, Smith & Brown (1990) investigated both forms of inviscid modes (i.e. the so-called acoustic and vorticity types) that may arise in a shock-free compressible boundary layer. For large values of the Mach number the vorticity mode is located at the edge of the boundary layer and is faster growing than the acoustic modes. The neutral curves corresponding to the two modes were delimited and it was shown that as the Mach number increases so the neutral curves become close. This near-linking of the neutral modes was investigated analytically and it was demonstrated that the separation distance between them actually becomes exponentially small with Mach number. (A similar near-linking is detailed by Dando & Seddougui (1993) for unstable inviscid Görtler vortices in compressible boundary layers over a curved plate.)

The study of CH was continued by Blackaby, Cowley & Hall (1993) to consider the

† Permanent address (for correspondence): School of Mathematics and Statistics, University of Birmingham, Birmingham, B15 2TT, UK.

strong-interaction zone, near the leading edge, as well as the region far downstream for hypersonic flow over a flat plate. In the latter region the attached shock has no effect, whereas it has an indirect effect near the leading edge because its presence leads to a modification of the basic flow. This investigation concentrated on inviscid modes of instability and assumed Sutherland's viscosity law. A significant outcome of this work was the demonstration that previous studies based on Chapman's viscosity law had overestimated the growth rate of unstable vorticity modes.

The present study addresses the question of the stability of hypersonic flow over a slender cone when the attached shock and also the effects of curvature are taken into account. Although viscous modes may not always prove to constitute the fastest growing modes, they will often nonetheless be important. An instance of this significance arises should the disturbance be triggered by wall roughness. The instability of the boundary layer on a cone to viscous modes may be described by a triple-deck structure in a similar way to that described by Duck & Hall (1989, 1990, hereafter referred to as DH1 and DH2) respectively. These articles considered the stability of supersonic flow over axisymmetric bodies to axisymmetric and non-axisymmetric disturbances. Curvature effects are unimportant unless the radius at the point of interest is much larger than the boundary layer thickness (see Duck 1984). When curvature effects are significant, the results of DH1 and DH2 show that the neutral curves bear no resemblance to those in the absence of curvature. These results may easily be generalized for hypersonic flows and the details of this aspect are given. It is noted that the axisymmetric modes actually form a distinguished family of modes, for in this eventuality the Mach number can be completely scaled out from the relevant stability equations.

The inviscid stability analysis for axisymmetric disturbances to supersonic flow along a circular cylinder considered by Duck (1990) showed that the effect of curvature was stabilizing. This study was extended by Duck & Shaw (1990) to consider non-axisymmetric disturbances to the flow over a sharp cone. They considered temporal growth rates of inviscid modes and identified an additional mode of instability which may be the most unstable. Asymptotic analysis presented in the limit of small or large distances downstream for disturbances with small wavenumbers indicates a link between this additional mode and the non-axisymmetric viscous mode described by DH2.

The stability of the laminar boundary layer over a sharp cone has been investigated experimentally by Stetson *et al.* (1983) for Mach 8 flow past a  $7^\circ$  half-angle cone. Disturbance amplification rates were measured and a stability diagram obtained which indicates the existence of multiple unstable regions in a hypersonic boundary layer. The experimental results of Fischer & Weinstein (1972) on a  $2.87^\circ$  half-angle cone with small nose radius at a Mach number of 18 revealed a wavy appearance of the boundary layer edge. The authors suggest that this instability could lead to transition to turbulence. The schlieren photographs presented show that the shock occurred far outside the boundary-layer region at this downstream location. Thus, this situation is not relevant to the present investigation where the shock is taken to be at the edge of the boundary layer.

Following the work of CH, Chang, Malik & Hussaini (1990) investigated the effects of a shock on the stability of hypersonic boundary layers on a wedge and a cone. A parallel-flow approach was used and computed growth rates were compared with those observed by Stetson *et al.* (1983). The authors concluded that the effect of the shock is not significant when it is located outside the edge of the boundary layer, and has a stabilizing influence when it is located near the edge of the boundary layer.

More recently, Pruett & Chang (1995) have conducted a direct numerical simulation of the experiments of Stetson *et al.* (1983). Here, however, the effect of any attached shock was neglected and instead attention was focused on the properties of three-dimensional second-mode waves.

The stability of the supersonic boundary layer on a rotating cone was investigated numerically by Balakumar & Reed (1991). They invoked Mangler's transformation (see for example, Stewartson 1964); this transformation has the effect of reducing the governing equations for an axisymmetric flow to the planar form. This work was primarily concerned with describing the effect of the three-dimensionality of the basic flow on its subsequent stability characteristics.

The influence of free-stream disturbances on a shock attached to a sharp cone has been investigated by Duck, Lasseigne & Hussaini (1995). Their analysis considered the whole region from the tip of the cone to distances far downstream, as opposed to the local analysis employed in the present paper. Here, in §2, the basic hypersonic flow over a sharp cone is described and, importantly, the conditions which must be satisfied at the shock are discussed. The linear stability of this basic flow is investigated in §3 following the triple-deck formulation used by CH, DH1 and DH2 for non-axisymmetric disturbances. Dispersion relationships for both axisymmetric and non-axisymmetric disturbances are derived in §4; in §5 neutral modes are obtained by numerical solution of these eigenrelations. These computations reveal that the behaviours of the neutral curves take on special forms if the shock is either far away from or close to the cone surface. We derive some asymptotic results for these two cases in §6 and show that there is good agreement between these and the numerical results obtained in §5.

Although neutral modes are of interest, in an experimental setting non-neutral disturbances are important. In the remainder of the article we discuss some properties of non-neutral modes, both axisymmetric and non-axisymmetric types. In §7 we concentrate on the question of temporal instabilities whilst in §8 attention is focused on the spatial problem. Finally, in §9, we draw a few conclusions.

## 2. Formulation

The flow of a compressible viscous fluid over a sharp cone of semi-angle  $\theta_c$  is considered at hypersonic speeds, with magnitude  $U_0$  parallel to its axis. We consider an attached shock which makes an angle  $\theta_s$  with the cone; a situation which is illustrated in figure 1. Spherical polars  $(x, \theta, \phi)$  is the natural coordinate system in which to describe the basic flow, and here  $\phi$  denotes the azimuthal angle. Furthermore, the radial distance  $x$  has been non-dimensionalized with respect to  $L^*$ , the distance from the tip of the cone to the location under consideration.

If viscous effects are neglected the fluid velocities  $(\bar{u}, \bar{v}, \bar{w})$ , pressure,  $\bar{p}$ , and density,  $\bar{\rho}$ , satisfy the continuity and (inviscid) Euler equations, namely

$$\frac{\partial \bar{\rho}}{\partial t} + \frac{1}{x^2 \sin \theta} \left[ \frac{\partial}{\partial x} (x^2 \sin \theta \bar{\rho} \bar{u}) + \frac{\partial}{\partial \theta} (x \sin \theta \bar{\rho} \bar{v}) + \frac{\partial}{\partial \phi} (x \bar{\rho} \bar{w}) \right] = 0, \quad (2.1a)$$

$$\bar{\rho} \frac{D\bar{u}}{Dt} - \frac{\bar{\rho} \bar{v}^2}{x} - \frac{\bar{\rho} \bar{w}^2}{x} = -\frac{\partial \bar{p}}{\partial x}, \quad (2.1b)$$

$$\bar{\rho} \frac{D\bar{v}}{Dt} + \frac{\bar{\rho} \bar{u} \bar{v}}{x} - \frac{\bar{\rho} \bar{w}^2 \cos \theta}{x \sin \theta} = -\frac{1}{x} \frac{\partial \bar{p}}{\partial \theta}, \quad (2.1c)$$

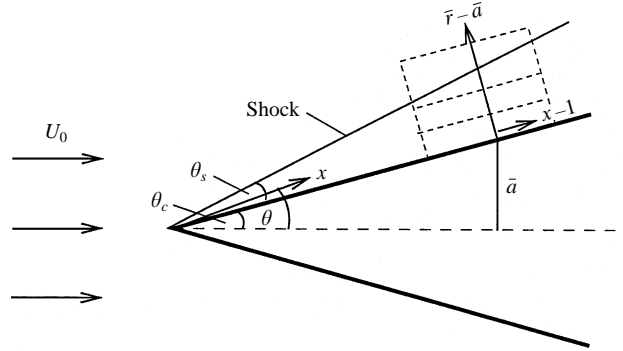


FIGURE 1. The geometry of the cone and shock. The cone is taken to be of semi-angle  $\theta_c$  with the attached shock making an angle  $\theta_s$  with the surface of the cone. Our study is concerned with the stability of the flow at a location distance  $L^*$  along the cone surface; i.e. where  $x = 1$ . In the triple-deck structure located at  $x = 1$  the coordinate  $\bar{r}$  (see below (2.10)) defines distance normal to the cone surface. When  $x = 1$  the cone radius  $a^*$  ( $= \sin \theta_c$ )  $= \bar{a}L^*$  where the dimensionless radius  $\bar{a} = O(M^{-1/4}Re^{-3/8}\mu_w^{3/8}T_w^{-9/8})$ , see §3.

$$\frac{D\bar{w}}{Dt} + \frac{\bar{\rho}\bar{w}\bar{u}}{x} + \frac{\bar{\rho}\bar{w}\bar{v}\cos\theta}{x\sin\theta} = -\frac{1}{x\sin\theta}\frac{\partial\bar{p}}{\partial\phi}, \tag{2.1d}$$

$$\bar{\rho}\gamma\frac{D}{Dt}\left(\frac{\bar{p}}{\bar{\rho}}\right) = (\gamma - 1)\frac{D\bar{p}}{Dt}, \tag{2.1e}$$

where

$$\frac{D}{Dt} \equiv \frac{\partial}{\partial t} + \bar{u}\frac{\partial}{\partial x} + \frac{\bar{v}}{x}\frac{\partial}{\partial\theta} + \frac{\bar{w}}{x\sin\theta}\frac{\partial}{\partial\phi},$$

and  $\gamma = c_p/c_v$  is the ratio of specific heats of the fluid.

The velocities are non-dimensionalized with respect to  $U_-$ , where  $U_-$  is the magnitude of the fluid velocity just behind the shock (see later). Throughout the paper, subscripts  $+$  and  $-$  respectively denote quantities just ahead of and just behind the shock. Additionally, the time  $t$ ,  $\bar{p}$ , and  $\bar{\rho}$ , have been non-dimensionalized with respect to  $L^*/U_-$ ,  $\rho_-U_-^2$  and  $\rho_-$  respectively, where  $\rho_-$  is the density just behind the shock. Finally, the basic temperature  $\bar{T}$  has been non-dimensionalized by  $T_-$ , the temperature just behind the shock.

If  $\varepsilon \equiv \rho_+/\rho_-$ , the ratio between the fluid density just ahead of the shock and that just behind it, is sufficiently small, then the density can be taken as constant in the region between the shock and the cone. In this case the shock layer is thin, and the viscosity  $\mu$  may be taken as constant with  $\mu = \mu_-$ .

The steady constant-density solution of (2.1) is well-known (e.g. Hayes & Probstein 1966) and is best given in the form of a velocity potential

$$\Phi = x\frac{U_0}{U_-}[AP_1(z) + BQ_1(z)], \tag{2.2}$$

where  $P_1$  and  $Q_1$  are the Legendre functions

$$P_1(z) = z \quad \text{and} \quad Q_1(z) = \frac{z}{2}\ln\left(\frac{1+z}{1-z}\right) - 1.$$

Here  $z \equiv \cos\theta$  with  $\bar{u} = \partial\Phi/\partial x$  and  $\bar{v} = (1/x)\partial\Phi/\partial\theta$ . (Note that the flow is axisymmetric so  $w = 0$ .) The constants  $A$  and  $B$  in the solution between the shock and the cone are determined from the conditions at the shock which is located at

$\theta = \sigma$ , where  $\sigma = \theta_c + \theta_s$ . The radial component of velocity is constant across the shock and equals  $U_0 \cos \sigma / U_-$  there whilst the polar component of velocity is normal to the shock and satisfies  $v_+ = \varepsilon^{-1} v_- = -U_0 \sin \sigma / U_-$ . If the definition  $z_s \equiv \cos \sigma$  is made, then these shock conditions can be used to determine  $A$  and  $B$  so that

$$A = \varepsilon + (1 - \varepsilon)z_s(1 - z_s^2)Q_1'(z_s), \quad (2.3a)$$

and

$$B = -(1 - \varepsilon)z_s(1 - z_s^2), \quad (2.3b)$$

where

$$Q_1'(z) = Q_0(z) + \frac{z}{1 - z^2},$$

and  $Q_0$  is the Legendre function

$$Q_0(z) = \frac{1}{2} \ln \left( \frac{1+z}{1-z} \right).$$

Hence the solutions for  $\bar{u}$ ,  $\bar{v}$  and  $\bar{p}$  in the zone between the shock and the cone are

$$\bar{u} = (U_0/U_-)(AP_1(z) + BQ_1(z)), \quad (2.4a)$$

$$\bar{v} = -(U_0/U_-)(1 - z^2)^{1/2}(A + BQ_1'(z)), \quad (2.4b)$$

and

$$\begin{aligned} \frac{U_-^2}{U_0^2} \bar{p} = & \frac{1}{2\gamma} \varepsilon(1 + \varepsilon) \sin^2 \sigma \\ & - \left[ ABQ_0(z) + \frac{B^2}{2} \left( Q_0^2(z) + \frac{1}{1 - z^2} \right) + \frac{A^2}{2} - \frac{\varepsilon}{2}(1 - z_s^2) - \frac{z_s^2}{2} \right]. \end{aligned} \quad (2.4c)$$

One significant feature of this solution is that the velocities are not uniform in the region between the shock and the cone, which is in direct contrast to the corresponding basic flow over a wedge. This has important consequences in the following analysis but, somewhat fortuitously, it does not prevent progress being made.

The jump conditions at the shock determine the relationships between  $\rho_+$  and  $\rho_-$  and  $p_+$  and  $p_-$ . These are given in Hayes & Probstein (1966) for any flow in terms of the Mach number of the oncoming flow normal to the shock,  $M_n$ , where  $M_n = U_0 v_+ / a_+$  with  $a_+$  denoting the speed of sound given by

$$a_+^2 = \gamma p_+ / \rho_+ \quad (2.5a)$$

and  $\gamma$  defined to be the ratio of specific heats of the fluid. If the Mach number  $M_+$  of the flow just ahead of the shock is set to be

$$M_+ = U_0 / a_+, \quad (2.5b)$$

then this gives  $M_n = -M_+ \sin \sigma$ ,

$$\varepsilon = \left( \frac{\gamma - 1}{\gamma + 1} \right) \left( 1 + \frac{2}{(\gamma - 1)M_+^2 \sin^2 \sigma} \right), \quad (2.6a)$$

and

$$p_- / p_+ = 1 + \gamma M_+^2 \sin^2 \sigma (1 - \varepsilon). \quad (2.6b)$$

The magnitude of the fluid velocity just behind the shock is given by

$$U_- = (U_-^2 \bar{u}^2 + U_-^2 \bar{v}^2)^{1/2} = U_0 \cos \sigma (1 + \varepsilon^2 \tan^2 \sigma)^{1/2} \quad (2.7)$$

and this result can be used to determine the Mach number just behind the shock,  $M_-$ , as

$$M_-^2 = \frac{M_+^2 \cos^2 \sigma (1 + \varepsilon^2 \tan^2 \sigma)}{1 + \frac{1}{2}(\gamma - 1)(1 - \varepsilon^2)M_+^2 \sin^2 \sigma}, \quad (2.8a)$$

whilst

$$M_+^2 = \frac{M_-^2}{\cos^2 \sigma (1 + \varepsilon^2 \tan^2 \sigma) - \frac{1}{2}(\gamma - 1)(1 - \varepsilon^2)M_-^2 \sin^2 \sigma}. \quad (2.8b)$$

Furthermore, for the angle between the shock and the cone,  $\tan \theta_s = -v_-/u_-$ , i.e.

$$\tan \theta_s = \varepsilon \tan \sigma. \quad (2.9)$$

Expressions (2.5)–(2.9) are the same as those given by CH but since the basic flow is not uniform now, they are only valid for quantities evaluated either just ahead of or just behind the shock.

The solutions for the basic flow (2.4) are not valid close to the surface of the cone and so a boundary-layer solution has to be introduced in this region. For the purposes of analysing this layer we define the Reynolds number of the flow by

$$Re = \rho_- U_- L^* / \mu_-. \quad (2.10)$$

Since the angle of the cone is taken to be small and also the angle between the shock and the cone must be small (see later) the flow between the shock and the cone satisfies the continuity and Navier–Stokes equations in terms of non-dimensional coordinates  $(x, \bar{r}, \phi)$  where  $x$  and  $\phi$  are as defined previously and  $L^* \bar{r}$  is the normal direction to the cone surface, where  $\bar{r} = \bar{a}$  on the generator of the cone. Thus, neglecting terms of  $O(\theta_c)$ , the equations satisfied by the corresponding non-dimensional velocities  $(u, v, w)$  and the non-dimensionalized pressure and density  $p$  and  $\rho$  are

$$\frac{\partial \rho}{\partial t} + \frac{\partial}{\partial x}(\rho u) + \frac{1}{\bar{r}} \frac{\partial}{\partial \bar{r}}(\bar{r} \rho v) + \frac{1}{\bar{r}} \frac{\partial}{\partial \phi}(\rho w) = 0, \quad (2.11a)$$

$$\rho \frac{Du}{Dt} = -\frac{\partial p}{\partial x} + \frac{1}{Re} \left\{ \frac{\partial}{\partial x} \left[ 2\mu \frac{\partial u}{\partial x} + \left( \mu' - \frac{2\mu}{3} \right) \nabla \cdot \mathbf{u} \right] + \frac{1}{\bar{r}} \frac{\partial}{\partial \bar{r}} \left[ \mu \bar{r} \left( \frac{\partial v}{\partial x} + \frac{\partial u}{\partial \bar{r}} \right) \right] + \frac{1}{\bar{r}} \frac{\partial}{\partial \phi} \left[ \mu \left( \frac{1}{\bar{r}} \frac{\partial u}{\partial \phi} + \frac{\partial w}{\partial x} \right) \right] \right\}, \quad (2.11b)$$

$$\rho \left( \frac{Dv}{Dt} - \frac{w^2}{\bar{r}} \right) = -\frac{\partial p}{\partial \bar{r}} + \frac{1}{Re} \left\{ \frac{\partial}{\partial \bar{r}} \left[ 2\mu \frac{\partial v}{\partial \bar{r}} + \left( \mu' - \frac{2\mu}{3} \right) \nabla \cdot \mathbf{u} \right] + \frac{1}{\bar{r}} \frac{\partial}{\partial \phi} \left[ \mu \left( \frac{1}{\bar{r}} \frac{\partial v}{\partial \phi} + \frac{\partial w}{\partial \bar{r}} - \frac{w}{\bar{r}} \right) \right] + \frac{\partial}{\partial x} \left[ \mu \left( \frac{\partial v}{\partial x} + \frac{\partial u}{\partial \bar{r}} \right) \right] + \frac{2\mu}{\bar{r}} \left( \frac{\partial v}{\partial \bar{r}} - \frac{1}{\bar{r}} \frac{\partial w}{\partial \phi} - \frac{v}{\bar{r}} \right) \right\}, \quad (2.11c)$$

$$\rho \left( \frac{Dw}{Dt} + \frac{vw}{\bar{r}} \right) = -\frac{1}{\bar{r}} \frac{\partial p}{\partial \phi} + \frac{1}{Re} \left\{ \frac{1}{\bar{r}} \frac{\partial}{\partial \phi} \left[ \frac{2\mu}{\bar{r}} \frac{\partial w}{\partial \phi} + \left( \mu' - \frac{2\mu}{3} \right) \nabla \cdot \mathbf{u} \right] + \frac{\partial}{\partial x} \left[ \mu \left( \frac{1}{\bar{r}} \frac{\partial u}{\partial \phi} + \frac{\partial w}{\partial x} \right) \right] + \frac{\partial}{\partial \bar{r}} \left[ \mu \left( \frac{1}{\bar{r}} \frac{\partial v}{\partial \phi} + \frac{\partial w}{\partial \bar{r}} - \frac{w}{\bar{r}} \right) \right] + \frac{2\mu}{\bar{r}} \left( \frac{1}{\bar{r}} \frac{\partial v}{\partial \phi} + \frac{\partial w}{\partial \bar{r}} - \frac{w}{\bar{r}} \right) \right\}, \quad (2.11d)$$

where

$$\frac{D}{Dt} \equiv \frac{\partial}{\partial t} + u \frac{\partial}{\partial x} + v \frac{\partial}{\partial \bar{r}} + \frac{w}{\bar{r}} \frac{\partial}{\partial \phi}$$

and

$$\nabla \cdot \mathbf{u} \equiv \frac{\partial u}{\partial x} + \frac{1}{\bar{r}} \frac{\partial}{\partial \bar{r}}(\bar{r}v) + \frac{1}{\bar{r}} \frac{\partial w}{\partial \phi},$$

where the viscosities,  $\mu$  and  $\mu'$ , have been non-dimensionalized with respect to  $\mu_-$ . The equation for the temperature  $T$  is

$$\begin{aligned} \rho \frac{DT}{Dt} = (\gamma - 1)M_-^2 \frac{Dp}{Dt} + \frac{1}{PrRe} \left[ \frac{\partial}{\partial x} \left( \mu \frac{\partial T}{\partial x} \right) + \frac{1}{\bar{r}} \frac{\partial}{\partial \bar{r}} \left( \bar{r}\mu \frac{\partial T}{\partial \bar{r}} \right) + \frac{1}{\bar{r}^2} \frac{\partial}{\partial \phi} \left( \mu \frac{\partial T}{\partial \phi} \right) \right] \\ + \frac{(\gamma - 1)M_-^2}{Re} \Phi_T, \end{aligned} \quad (2.11e)$$

where

$$\begin{aligned} \Phi_T \equiv 2\mu \left[ \left( \frac{\partial u}{\partial x} \right)^2 + \left( \frac{\partial v}{\partial \bar{r}} \right)^2 + \left( \frac{1}{\bar{r}} \frac{\partial w}{\partial \phi} + \frac{v}{\bar{r}} \right)^2 + \frac{1}{2} \left( \frac{\partial u}{\partial \phi} + \frac{\partial w}{\partial x} \right)^2 + \frac{1}{2} \left( \frac{\partial v}{\partial x} + \frac{\partial u}{\partial \bar{r}} \right)^2 \right. \\ \left. + \frac{1}{2} \left( \frac{1}{\bar{r}} \frac{\partial v}{\partial \phi} + \frac{\partial w}{\partial \bar{r}} - \frac{w}{\bar{r}} \right)^2 \right] + \left( \mu' - \frac{2\mu}{3} \right) (\nabla \cdot \mathbf{u})^2, \end{aligned}$$

$M_-^2 = U_-^2/((\gamma - 1)c_p T_-)$ , and  $Pr$  is the Prandtl number. If the fluid is assumed to be a perfect gas then the equation of state becomes

$$\gamma M_-^2 p = \rho T. \quad (2.11f)$$

The relevant boundary conditions are  $u = v = w = 0$  and  $T = T_w$  at the surface of the cone, together with appropriate conditions at the shock location (see later) given by  $\bar{r} = \bar{r}_s$ , say.

In the following analysis it is found that we do not need to be precise about the boundary condition for the temperature at the surface of the cone; the only restriction that must be imposed is that  $T_w \gg 1$ . This will be the case for an adiabatic wall, where there is no heat transfer at the surface, as well as for an isothermal wall for which the temperature of the surface is maintained at a prescribed constant value. The only circumstance when the assumption  $T_w \gg 1$  is no longer valid arises when strong cooling is applied to the cone surface. Studies of the effects of severe cooling include those by Seddougui, Bowles & Smith (1991) for general compressible flows and investigations by Brown, Cheng & Lee (1990) and Kerimbekov, Ruban & Walker (1994) for hypersonic flows. Hereafter we shall suppose that  $T_w = T_b T_r$  where  $T_r$  is the adiabatic wall temperature given by  $T_r = 1 + (\gamma - 1)M_-^2/2$  where  $M_- \equiv M$ .

It is noteworthy that the subsequent analysis in the current paper is unaffected by the choice of the underlying viscosity law relating the fluid viscosity to its temperature. In their study CH derived restrictions on the various parameters in their problem in order to ensure that the analysis is valid if Chapman's law or the more accurate Sutherland's law is assumed. These restrictions arise from the constraints that the shock should lie within the upper tier of the governing triple-deck structure outlined below and that the wavelength of the Tollmien-Schlichting waves is much less than the distance from the apex of the cone. For Chapman's law  $\mu_w = CT_w$ , our subsequent

analysis is valid for

$$M \sim \sigma^{8/7} Re^{3/14}, \quad Re^{-1/10} \leq \sigma \leq Re^{-1/122}, \quad (2.12a)$$

whilst for Sutherland's relation  $\mu_w \sim (1 + \bar{C})T_w^{1/2}$  we require

$$M \sim \sigma^{13/14} Re^{3/14}, \quad Re^{-1/9} \leq \sigma \leq Re^{-1/107}; \quad (2.12b)$$

these inequalities also ensure that the lower-deck analysis will be linear. Finally, the precise value of the Prandtl number taken in our work is not significant. However, it should be cautioned that the investigation of Grubin & Trigub (1993) revealed the importance of the values of  $Pr$  and  $\omega$  for the long-wave limit of inviscid modes, where  $\omega$  is the exponent in the viscosity power law  $\mu_w \propto T_w^\omega$ . Thus, in order to connect our results for viscous modes to other disturbance types in an appropriate limit, it may be important to assign values to  $Pr$  and  $\omega$ .

### 3. The stability problem

The linear stability of the basic flow described above for  $M \gg 1$  and  $Re \gg 1$  is investigated in the weak-interaction region following the triple-deck formulation used by CH, DH1 and DH2. The conditions to be satisfied at the shock by a disturbance to this basic flow must be specified and these are derived in detail by Seddougui (1994). The requisite constraints were obtained by considering the linearized jump conditions at the shock for infinitesimal waves beneath the shock; a similar procedure was adopted by CH for flow over a wedge. Although the basic flow is not uniform in the regions below and above the shock, Seddougui (1994) showed that the jump conditions may still be evaluated at the undisturbed position of the shock. Furthermore, the linear waves between the shock and the cone have different forms than those for a wedge. The condition satisfied by the pressure amplitudes of the two acoustic waves (which are incident and reflected from the shock) is found to be similar to that obtained by CH.

Attention is focused at a location on the surface of the cone with non-dimensional radius  $\bar{a} = a^*/L^*$ . It is assumed that  $\bar{a}Re^{3/8}M^{1/4}\mu_w^{-3/8}T_w^{-9/8} \sim O(1)$  denotes the scale of the radius at this point; thus we have chosen  $\sin \theta_c \sim \theta_c \sim Re^{-3/8}M^{-1/4}\mu_w^{3/8}T_w^{9/8}$ .

Our study is confined to the question of the stability of the flow at a location on the body where the boundary-layer thickness is  $O(Re^{-1/2}L^*)$ , which is thin compared to the local radius of the cone. This situation is chosen so that curvature effects are significant. The analysis is somewhat simplified if non-parallel effects can be neglected and CH showed that this is justifiable if the 'Newtonian' assumption  $\gamma - 1 \ll 1$  is made. Thus, for simplicity, this condition is taken to hold in the following analysis although it can be easily relaxed for more involved studies.

It is convenient to scale out some of the parameters in the problem, namely  $\mu_w$ ,  $T_w$  and  $\lambda$ , where the last quantity denotes the boundary-layer skin friction and throughout the subscript  $w$  is used to denote values at the surface of the cone. Following CH we introduce the scales

$$\left. \begin{aligned} x &= 1 + Re^{-3/8}\mu_w^{3/8}\lambda^{-5/4}T_w^{9/8}M^{3/4}X, & \bar{a} &= Re^{-3/8}\mu_w^{3/8}\lambda^{-5/4}T_w^{9/8}M^{-1/4}a, \\ t &= Re^{-1/4}\mu_w^{1/4}\lambda^{-3/2}T_w^{3/4}M^{1/2}\tau. \end{aligned} \right\} \quad (3.1)$$

In the lower tier of the triple-deck structure, where viscous effects are important,



we have

$$\left. \begin{aligned} \bar{r} - \bar{a} &= Re^{-5/8} \mu_w^{5/8} \lambda^{-3/4} T_w^{7/8} M^{1/4} Y, & u &\sim Re^{-1/8} \mu_w^{1/8} \lambda^{1/4} T_w^{3/8} M^{1/4} U, \\ v &\sim Re^{-3/8} \mu_w^{3/8} \lambda^{3/4} T_w^{1/8} M^{-1/4} V, & w &\sim Re^{-1/8} \mu_w^{1/8} \lambda^{1/4} T_w^{3/8} M^{-3/4} W, \\ p &\sim \gamma^{-1} M^{-2} + Re^{-1/4} \mu_w^{1/4} \lambda^{1/2} T_w^{-1/4} M^{-3/2} P, & T &\sim T_w, \quad \rho \sim T_w^{-1}. \end{aligned} \right\} \quad (3.2)$$

Substituting these expressions into the non-dimensionalized continuity and Navier-Stokes equations gives, at leading order

$$\left. \begin{aligned} U_X + V_Y + (1/a)W_\phi &= 0, & P_Y &= 0, \\ U_\tau + UU_X + VU_Y + (W/a)U_\phi &= U_{YY}, \\ W_\tau + UW_X + VW_Y + (W/a)W_\phi &= -(1/a)P_\phi + W_{YY}. \end{aligned} \right\} \quad (3.3)$$

Note that there is no  $P_X$  term in the  $X$ -momentum equation and this is a consequence of our examining the hypersonic limit. The necessary boundary conditions are

$$U = V = W = 0 \quad \text{on} \quad Y = 0, \quad (3.4a)$$

$$U \rightarrow Y + A(X, \phi, \tau), \quad W \rightarrow D/Y \quad \text{as} \quad Y \rightarrow \infty, \quad (3.4b)$$

where  $A$  is a displacement function and  $D$  satisfies  $D_X = -P_\phi/a$ .

The solutions of the above equations must match with those in the main deck as  $Y \rightarrow \infty$ . Owing to the presence of the temperature adjustment layer (a logarithmically small layer required to reduce the temperature of the basic flow from its  $O(M^2)$  value close to the surface to its  $O(1)$  value at the edge of the boundary layer) the main deck is itself sub-divided into three further regions. The details of these sub-regions follow those of CH so, for the sake of brevity, will not be repeated here. In the boundary-layer region where the basic temperature  $\bar{T} \equiv \gamma M^2 \bar{p}/\bar{\rho}$  (from the perfect gas relation (2.11f)) is large, the scalings and solutions are

$$\left. \begin{aligned} \bar{r} - \bar{a} &= Re^{-1/2} \mu_w^{1/2} T_w^{1/2} y, & u &\sim \bar{U}_0(y) + Re^{-1/8} \mu_w^{1/8} \lambda^{-3/4} T_w^{3/8} M^{1/4} A \bar{U}_{0y}, \\ v &\sim -Re^{-1/4} \mu_w^{1/4} \lambda^{1/2} T_w^{-1/4} M^{-1/2} A_X \bar{U}_0, & w &\sim Re^{-1/4} \mu_w^{1/4} \lambda^{1/2} T_w^{-1/4} M^{-1/2} D/(\bar{U}_0 \bar{R}_0), \\ p &\sim Re^{-1/4} \mu_w^{1/4} \lambda^{1/2} T_w^{-1/4} M^{-3/2} P, & \rho &\sim \bar{R}_0(y) + Re^{-1/8} \mu_w^{1/8} \lambda^{-3/4} T_w^{3/8} M^{1/4} A \bar{R}_{0y}, \end{aligned} \right\} \quad (3.5)$$

where  $\bar{U}_0$  and  $\bar{R}_0$  are the non-dimensional velocity and density, respectively, of the basic flow.

In order that the effect of the shock may be considered the scalings are chosen so that the shock occurs in the upper deck of the triple-deck structure. This requires that  $\theta_s \sim \theta_c \sim Re^{3/16} M^{-23/8}$  for Chapman's viscosity law, or  $\theta_s \sim Re^{3/13} M^{-40/13}$  for Sutherland's law. The scalings here are

$$\left. \begin{aligned} \bar{r} &= Re^{-3/8} \mu_w^{3/8} \lambda^{-5/4} T_w^{9/8} M^{-1/4} r, & u &\sim 1 + Re^{-1/4} \mu_w^{1/4} \lambda^{1/2} T_w^{-1/4} M^{-3/2} \tilde{u}, \\ v &\sim Re^{-1/4} \mu_w^{1/4} \lambda^{1/2} T_w^{-1/4} M^{-1/2} \tilde{v}, & w &\sim Re^{-1/4} \mu_w^{1/4} \lambda^{1/2} T_w^{-1/4} M^{-1/2} \tilde{w}, \\ p &\sim Re^{-1/4} \mu_w^{1/4} \lambda^{1/2} T_w^{-1/4} M^{-3/2} \tilde{p}, & \rho &\sim 1 + Re^{-1/4} \mu_w^{1/4} \lambda^{1/2} T_w^{-1/4} M^{1/2} \tilde{\rho}. \end{aligned} \right\} \quad (3.6)$$

Substitution of these expressions into the governing disturbance equations yields

$$\left. \begin{aligned} \frac{\partial \tilde{p}}{\partial X} + \frac{\partial \tilde{v}}{\partial r} + \frac{\tilde{v}}{r} + \frac{1}{r} \frac{\partial \tilde{w}}{\partial \phi} &= 0, & \frac{\partial \tilde{u}}{\partial X} &= -\frac{\partial \tilde{p}}{\partial X}, \\ \frac{\partial \tilde{v}}{\partial X} &= -\frac{\partial \tilde{p}}{\partial r}, & \frac{\partial \tilde{w}}{\partial X} &= -\frac{1}{r} \frac{\partial \tilde{p}}{\partial \phi}, & \frac{\partial \tilde{p}}{\partial X} &= \frac{\partial \tilde{\rho}}{\partial X}, \end{aligned} \right\} \quad (3.7)$$

where the effect of curvature is now apparent. Eliminating  $\tilde{v}$  and  $\tilde{w}$  from the first of (3.7) gives

$$\frac{\partial^2 \tilde{p}}{\partial r^2} + \frac{1}{r} \frac{\partial \tilde{p}}{\partial r} + \frac{1}{r^2} \frac{\partial^2 \tilde{p}}{\partial \phi^2} - \frac{\partial^2 \tilde{p}}{\partial X^2} = 0. \tag{3.8}$$

From matching with the main deck, the boundary conditions are  $\tilde{p}_r = A_{XX}$  and  $\tilde{p} = P$  at  $r = a$ . The remaining boundary condition is applied at the shock. For the scales presented here (appropriate to acoustic waves) Seddougui (1994) has shown that the requisite constraint is that  $\tilde{p} = 0$  at the shock location, defined by  $r = r_s$ .

In order to analyse the linear stability of the above system of equations we consider perturbations proportional to  $E = \exp[i(\alpha X + n\phi - \Omega\tau)]$  where  $n$  is an integer  $\geq 0$ . The linearized equations in the lower deck may be solved giving the solutions for the perturbations in terms of the Airy function  $\text{Ai}$  (see Abramowitz & Stegun 1964). In the upper deck, where we define  $\tilde{p} = \hat{p}(r)E$ , the function  $\hat{p}$  satisfies the modified Bessel equation of order  $n$ , namely

$$\frac{d^2 \hat{p}}{dr^2} + \frac{1}{r} \frac{d\hat{p}}{dr} - \frac{n^2}{r^2} \hat{p} + \alpha^2 \hat{p} = 0. \tag{3.9}$$

The boundary conditions at  $r = a$  are now  $\hat{p}_r = -\alpha^2 \hat{A}$  and  $\hat{p} = \hat{P}$ , where  $(A, P) = (\hat{A}, \hat{P})E$  and  $\hat{p} = 0$  at  $r = r_s$ . Matching the upper-deck solutions of (3.9) to the lower-deck quantities leads to the desired eigenrelations, an operation we consider now.

**4. Dispersion relations for axisymmetric and non-axisymmetric modes**

The case of axisymmetric disturbances must be considered separately from the non-symmetric ones, as in the former case the Mach number can be completely scaled out of the linear stability problem. Thus, the Mach number scales presented in the previous section are only strictly appropriate to non-axisymmetric disturbances.

For axisymmetric disturbances the pressure perturbation in the upper deck satisfies (3.9) with  $n = 0$ , although  $r$ ,  $\hat{p}$  and  $\hat{A}$  are scaled differently with respect to  $M$  to the variables defined in §3 (in fact, they have factors of powers of  $M^2 - 1$ ). The solution for  $\hat{p}$ , say  $\hat{p}_A$ , in this case is

$$\hat{p}_A(r) = i\alpha \hat{A} \frac{I_0(i\alpha r_s)K_0(i\alpha r) - I_0(i\alpha r)K_0(i\alpha r_s)}{I_0(i\alpha r_s)K'_0(i\alpha a) - I'_0(i\alpha a)K_0(i\alpha r_s)}, \tag{4.1}$$

where  $K_0(i\alpha r)$  and  $I_0(i\alpha r)$  are the usual modified Bessel functions. In the lower deck, satisfying the boundary condition for the disturbance along the cone as  $Y \rightarrow \infty$  and at  $Y = 0$  yields the condition

$$\frac{\text{Ai}'(\xi_0)}{\int_{\xi_0}^{\infty} \text{Ai}(\xi) d\xi} = (i\alpha)^{1/3} \frac{\hat{P}}{\hat{A}}, \tag{4.2}$$

where  $\xi = \xi_0 + (i\alpha)^{1/3} Y$  and  $\xi_0 = -i^{1/3} \Omega \alpha^{-2/3}$ . Hence, applying the condition  $\hat{p}(a) = \hat{P}$  yields an eigenrelation relating the streamwise wavenumber  $\alpha$  and frequency  $\Omega$ , namely

$$\frac{\text{Ai}'(\xi_0)}{\int_{\xi_0}^{\infty} \text{Ai}(\xi) d\xi} = -(i\alpha)^{4/3} \frac{I_0(i\alpha r_s)K_0(i\alpha a) - I_0(i\alpha a)K_0(i\alpha r_s)}{I_0(i\alpha r_s)K_1(i\alpha a) + I_1(i\alpha a)K_0(i\alpha r_s)}. \tag{4.3}$$

Before discussing some solutions of (4.3) it is useful to consider the corresponding eigenrelation obtained by DH1 in the absence of a shock. This is because inspection of (4.3) as  $r_s \rightarrow \infty$  reveals that, in the case of neutral modes, the eigenrelation does not tend to that obtained by DH1, as one might expect. If no shock is present then the solution of (3.9) with  $n = 0$  is proportional to  $K_0(i\alpha r)$ , allowing only for outgoing waves as  $r \rightarrow \infty$ . The requisite details are given in DH1 and the appropriate eigenrelation has the form

$$\frac{\text{Ai}'(\xi_0)}{\int_{\xi_0}^{\infty} \text{Ai}(\xi) d\xi} = -(\text{i}\alpha)^{4/3} \frac{K_0(\text{i}\alpha a)}{K_1(\text{i}\alpha a)}, \tag{4.4}$$

where  $\lambda$  has been scaled out in the manner described in §3.

4.1. Non-axisymmetric modes

For  $n > 0$  we find that the appropriate solution of (3.9) is given by

$$\hat{p}(r) = -\text{i}\alpha \hat{A} \frac{I_n(\text{i}\alpha r_s) K_n(\text{i}\alpha r) - I_n(\text{i}\alpha r) K_n(\text{i}\alpha r_s)}{I'_n(\text{i}\alpha a) K_n(\text{i}\alpha r_s) - I_n(\text{i}\alpha r_s) K'_n(\text{i}\alpha a)}. \tag{4.5}$$

The condition to be satisfied by  $\hat{P}$  from the lower-deck solution is now

$$\frac{\text{Ai}'(\xi_0)}{\int_{\xi_0}^{\infty} \text{Ai}(\xi) d\xi} = (\text{i}\alpha)^{-2/3} \frac{\text{i}n^2 \hat{P}}{\alpha a^2 \hat{A}} \tag{4.6}$$

and thus setting  $\hat{p}(a) = \hat{P}$  yields the eigenrelation

$$\frac{\text{Ai}'(\xi_0)}{\int_{\xi_0}^{\infty} \text{Ai}(\xi) d\xi} = (\text{i}\alpha)^{4/3} \frac{n^2}{\alpha^2 a^2} \frac{I_n(\text{i}\alpha r_s) K_n(\text{i}\alpha a) - I_n(\text{i}\alpha a) K_n(\text{i}\alpha r_s)}{I_n(\text{i}\alpha r_s) K'_n(\text{i}\alpha a) - I'_n(\text{i}\alpha a) K_n(\text{i}\alpha r_s)}. \tag{4.7}$$

As in the axisymmetric case discussed above, eigenrelation (4.7), when solved for neutral disturbances as  $r_s \rightarrow \infty$ , does not collapse to the hypersonic limit of DH2 in the absence of a shock. If no shock is present the corresponding eigenrelation is

$$\frac{\text{Ai}'(\xi_0)}{\int_{\xi_0}^{\infty} \text{Ai}(\xi) d\xi} = (\text{i}\alpha)^{4/3} \frac{n^2}{\alpha^2 a^2} \frac{K_n(\text{i}\alpha a)}{K'_n(\text{i}\alpha a)} \tag{4.8}$$

and the solution of (4.8) is shown in figure 2 for neutral values  $\alpha = \alpha(a)$  for  $n = 1-4$ . For any prescribed azimuthal wavenumber  $n$ , modes lying in the parameter space to the left of the corresponding neutral curve are unstable whilst those to the right are stable. This would seem to suggest that the instability region grows with  $n$  and so there is no sensible definition of the most dangerous mode. However, this view of the relative importances of the various modes disregards the size of the growth rates of the disturbances. In practice, it is reasonable to suppose that the significance of a particular mode is closely allied to its growth rate and we shall compute a selection of such amplification values later.

The form of solutions for  $\Omega$  corresponding to neutral modes is very similar to those presented for  $\alpha$  and the asymptotic behaviour of (4.8) for  $a \ll 1$  is derived in §6.1. We

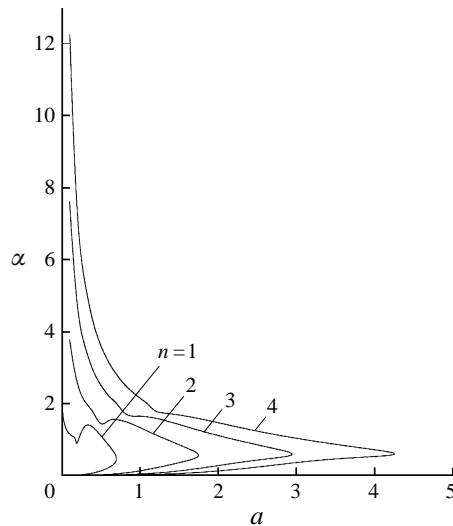


FIGURE 2. Neutral non-axisymmetric modes as given by solution of (4.8) for flow over the cone in the absence of the shock. Shown are the modes with azimuthal wavenumbers  $n = 1-4$ .

note that in the limit  $|\alpha a| \gg 1$  and  $n \gg 1$ , for  $\alpha^2 a^2 < n^2$  the eigenrelation reduces to

$$1.001 \left( 1 - \frac{\alpha^2 a^2}{n^2} \right)^{1/2} \approx \alpha^{1/3} \frac{n}{a}$$

and taking this limit corresponds to lessening the influence of curvature. Indeed, if we now write  $\beta = n/a$  then we retrieve the hypersonic planar relation of Smith (1989) which governs the stability of viscous flow over a flat plate. However, if the presence of the shock is taken into account, the situation is very different.

## 5. Neutral modes

We now consider neutrally stable solutions of dispersion relations (4.3) and (4.7) corresponding to the axisymmetric and non-axisymmetric cases respectively. As in the preceding section, we shall start by examining the axisymmetric relationship (4.3). The presence of the shock allows for multiple modes of solutions and it is convenient to write the modified Bessel functions in terms of  $J_n$  and  $Y_n$ . Thus (4.3) may be written as

$$\frac{\text{Ai}'(\xi_0)}{\int_{\xi_0}^{\infty} \text{Ai}(\xi) d\xi} = i^{1/3} \alpha^{4/3} \frac{J_0(\alpha r_s) Y_0(\alpha a) - J_0(\alpha a) Y_0(\alpha r_s)}{J_0(\alpha r_s) Y_1(\alpha a) - J_1(\alpha a) Y_0(\alpha r_s)}. \quad (5.1)$$

Real values of  $\alpha$  corresponding to the first ten modes satisfying (5.1) are shown in figure 3 with the shock location chosen at  $r_s = 1$ . In this figure the region of instability lies above the curves and, for larger values of  $a$ ,  $\alpha$  increases monotonically with  $a$ ; see figure 4 which illustrates this phenomenon for the first four modes. These neutral curves differ fundamentally from those obtained from (4.4) by DH1, where solutions are only possible for a finite range of  $a$  with  $a$  less than approximately 0.003. In that shockless problem when  $a \rightarrow 0$  the neutral solutions of (4.4) have  $\alpha$  (and  $\Omega$ ) tending to infinity for both the lower and upper branches: the precise asymptotic expressions are detailed in DH1. In the present case it appears that neutral solutions are possible

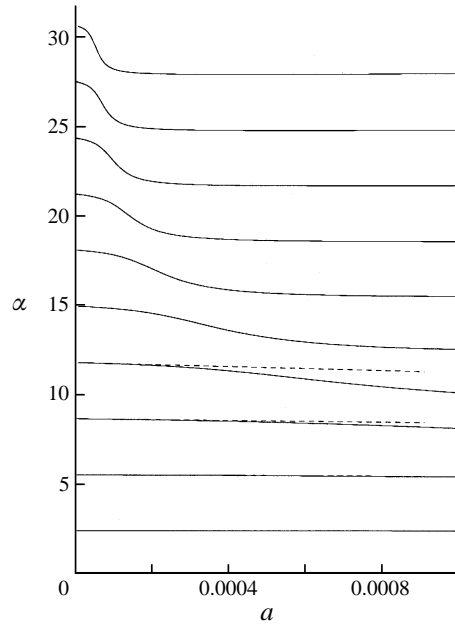


FIGURE 3. The first ten axisymmetric neutral modes giving the wavenumber  $\alpha$  in terms of the local cone radius  $0 < a < 0.001$  for shock position  $r_s = 1$ . Shown dashed are the small- $a$  asymptotic results as given by (6.2).

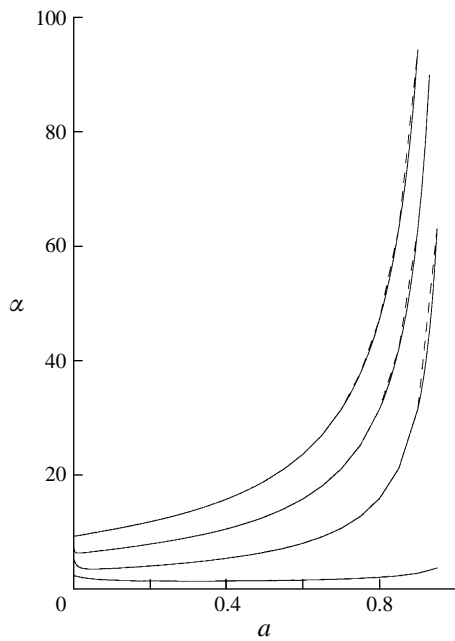


FIGURE 4. The first four axisymmetric neutral modes for  $r_s = 1$  and cone radius  $0 < a < 1$ . Shown dashed are the  $a \rightarrow r_s$  asymptotic results (6.9).

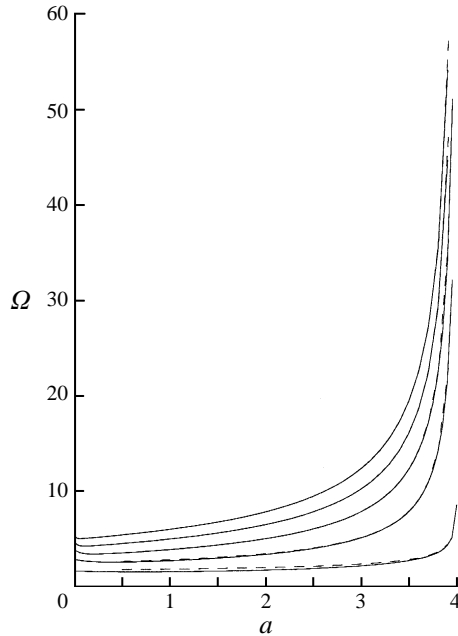


FIGURE 5. Neutral values of the frequency  $\Omega$  for the first five axisymmetric modes with  $r_s = 4$  and  $0 < a < 4$ . The  $a \rightarrow r_s$  asymptotic results (6.8) and (6.9) (with  $\Omega \approx 2.297\alpha^{2/3}$ ) are superimposed.

for all physically sensible values of  $a$ . (The upper limit on  $a$ , that is  $r_s$ , must be imposed or else we are in the absurd situation when the shock would lie inside the cone.) With the shock present we see from figure 3 that  $\alpha$  no longer grows indefinitely in the limit of zero cone radius as in DH1, but instead the neutral values tend to  $O(1)$  constants in this limit. Thus it appears that the stability of the flow over the cone to axisymmetric disturbances is significantly altered by the presence of the shock but figure 3 does contain a remnant of the neutral curve obtained by DH1. The kinking feature which develops in the higher modes of figure 3 at small values of  $a$  delimits a mode very reminiscent of the type identified by DH1; a brief justification of this assertion appears within our asymptotic analysis of §6.

For neutral solutions of (5.1), as in the classic planar incompressible stability problem, it is found that  $\xi_0 \approx -2.297i^{1/3}$  giving  $\Omega \approx 2.297\alpha^{2/3}$ . Thus, the neutral curves in  $\Omega$ -space have similar behaviours to those for  $\alpha$ . To take an example, neutral values of  $\Omega$  are shown in figure 5 for the first five modes associated with the shock position  $r_s = 4$ . Figure 6(a,b) shows neutral curves of  $\alpha$  from (5.1) for  $r_s = 4$  and  $r_s = 16$ , respectively, for the first five modes. Although not obvious from this figure, refined calculations for small  $a$  prove that the kinks evident in figure 3 continue to exist for the higher modes at these larger values of  $r_s$ . We see that as the shock moves away from the boundary layer, for fixed values of  $a$ , the neutral values of  $\alpha$  decrease. Thus, the shock appears to have a destabilizing effect since its distance from the surface increases as the area above the neutral curves is increased and growing solutions will be possible for a larger range of  $a$ . Finally, also shown on figures 3–6 are the asymptotic results described in §6 for the particular limits  $a \rightarrow 0$  and  $a \rightarrow r_s$ . The agreement is remarkably good in all cases.

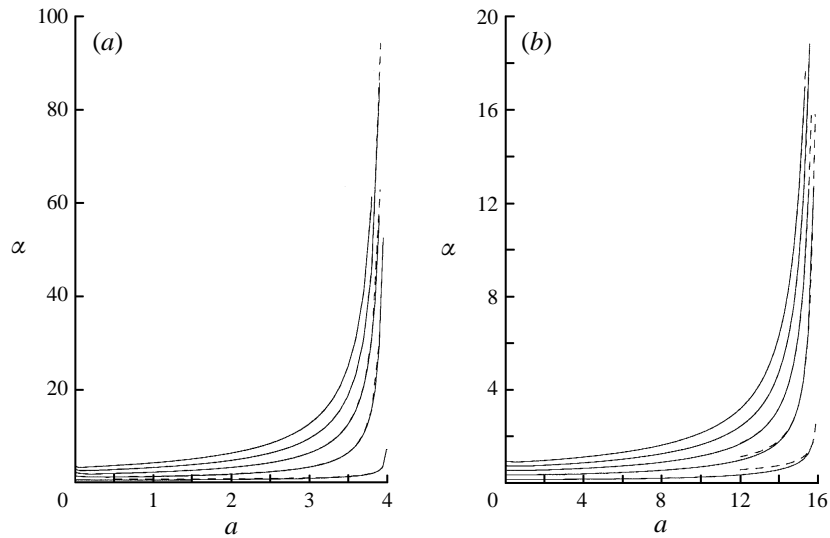


FIGURE 6. The first five axisymmetric neutral modes giving  $\alpha$  as a function of  $a$  for  $0 < a < r_s$  with (a)  $r_s = 4$ ; (b)  $r_s = 16$ . The  $a \rightarrow r_s$  asymptotic results (6.8) and (6.9) are indicated by broken lines.

5.1. Neutral non-axisymmetric disturbances

As in the axisymmetric case it is convenient to write the eigenrelation (4.7) in terms of  $J_n$  and  $Y_n$  so that

$$\frac{\text{Ai}'(\xi_0)}{\int_{\xi_0}^{\infty} \text{Ai}(\xi) d\xi} = i^{1/3} \alpha^{4/3} \frac{n^2}{\alpha^2 a^2} \frac{J_n(\alpha a) Y_n(\alpha r_s) - J_n(\alpha r_s) Y_n(\alpha a)}{J_n(\alpha r_s) Y_n'(\alpha a) - J_n'(\alpha a) Y_n(\alpha r_s)}. \tag{5.2}$$

Neutral solutions of (5.2) are shown in figure 7(a,b) for  $n = 1$  and  $r_s = 1$  and  $r_s = 4$ , respectively, and a number of remarks should be made concerning the forms of these curves. The first is that, unlike the axisymmetric case, there are no kinks on the curves for small values of  $a$  for higher modes. For small values of  $a$ , with the exception of the first mode, the neutral value of  $\alpha$  tends to a non-zero constant, as in the axisymmetric case, although for  $r_s = 1$  the minimum value now occurs as  $a \rightarrow 0$  (cf. figure 4 which clearly shows that in the axisymmetric problem the minimum value of  $\alpha$  corresponds to a non-zero body radius). The first mode on figure 7(a,b) has  $\alpha$  tending to zero as  $a \rightarrow 0$  which corresponds to the solutions in the absence of a shock (see figure 2). The asymptotic behaviour for  $a \rightarrow r_s$  is the same for all modes and is described in §6.2, with the corresponding behaviour for  $a \rightarrow 0$  given in §6.1. The asymptotic results shown on figure 7 illustrate a very close agreement with the computed results. For larger values of  $r_s$  the neutral curves all move closer to the  $a$ -axis for fixed  $n$ , as illustrated by figure 7(b). Further calculations show that the asymptotic expressions of §6.2 continue to give excellent agreement for larger values of  $r_s$  and  $n$ . Figure 8 gives the solution for  $\alpha$  with  $n = 2$  and  $r_s = 1$ . We find that as  $n$  increases for fixed  $r_s$  the solutions do not alter significantly, particularly as  $a \rightarrow r_s$ . However, it is worth noting that for the first-mode solution the neutral values of  $\alpha$  decrease as  $n$  increases: the significance of this is discussed in DH2. Figure 9 shows neutral values of  $\alpha$  for  $r_s = 16$  and  $n = 1$  and  $n = 2$  but in order to illustrate the behaviour of the solution

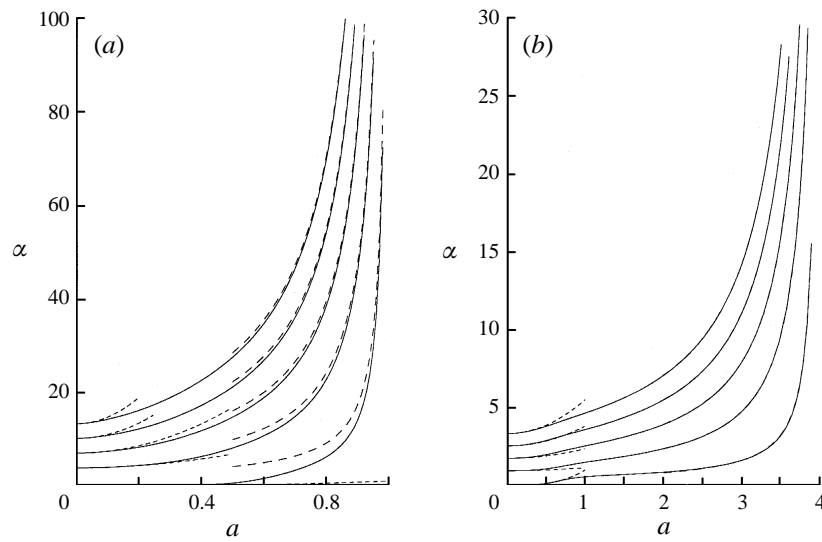


FIGURE 7. The first five neutral modes with azimuthal wavenumber  $n = 1$ . Shown is  $\alpha$  against  $a$  for  $0 < a < r_s$  and (a)  $r_s = 1$ ; (b)  $r_s = 4$ . The small  $a$  and  $a \rightarrow r_s$  asymptotes as given by (6.4) and (6.10) are also indicated. Note that the  $a \rightarrow r_s$  asymptotes in (b) are indistinguishable from the computed solutions.

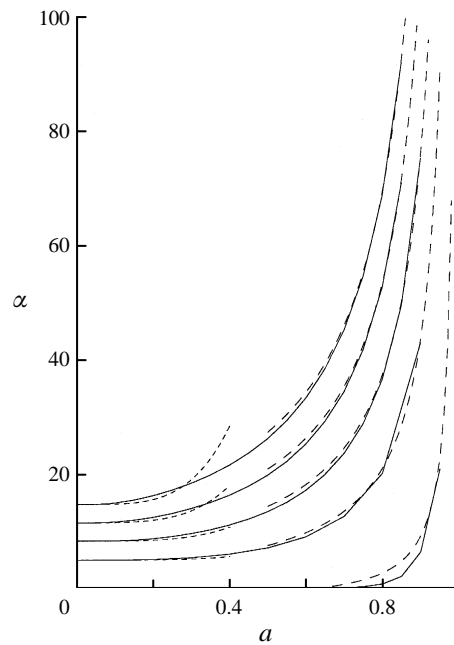


FIGURE 8. The first five neutral modes with azimuthal wavenumber  $n = 2$  and shock location  $r_s = 1$ .

curves for small  $a$  the results shown are restricted to  $a \leq 10$ . For small values of  $a$  the first-mode solution does not feel the influence of the shock and has a behaviour similar to the solutions of (4.8) (see figure 2). However, as  $a$  increases so the shock has an increasingly dramatic effect on the solution.



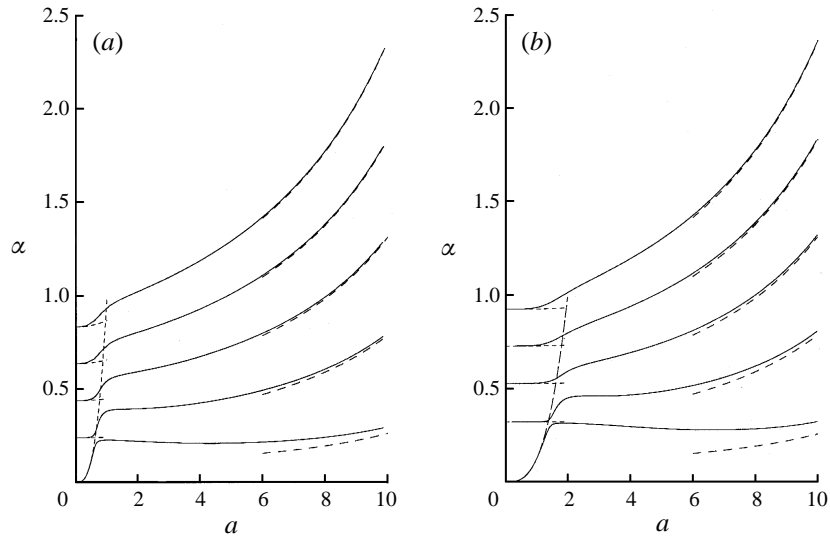


FIGURE 9. The first five neutral modes with azimuthal wavenumbers (a)  $n = 1$ ; (b)  $n = 2$ . The shock is located at  $r_s = 16$  and, in order to clarify the solution behaviours for small  $a$ , the horizontal axis is restricted to  $0 < a < 10$ . We remark that the  $a \rightarrow r_s$  asymptotes are very accurate for  $a$  greater than about 8.

**6. Asymptotic solutions of the eigenrelations**

Before discussing some non-neutral solutions of the dispersion relations, it is useful to consider some asymptotic solutions of (5.1) and (5.2) in the limits of small  $a$  and large  $a$ .

6.1. *Limit as  $a \rightarrow 0$ .*

As  $a \rightarrow 0$  (with the exception of the first mode for  $n > 0$ ) the numerical results suggest that  $\alpha$  and  $\Omega$  tend to non-zero constants. This can be confirmed analytically as follows. Examination of the structures of the respective eigenrelations (5.1) and (5.2) in terms of  $J_n$  and  $Y_n$ , suggests that if  $\alpha a \ll 1$  then the  $Y_n$  terms are likely to dominate the  $J_n$  ones. In order to check this, we approximate the left-hand sides of (5.1) and (5.2) by  $1.001i^{1/3}$  so that we anticipate the result that  $\xi_0 \approx 2.297i^{1/3}$  as in the classical work. On substitution of the series expansions of  $J_n$  and  $Y_n$  into the approximate eigenrelations, with  $\alpha = \alpha_0 + a^p \alpha_1 + \dots$  and  $p$  to be fixed, we find that to achieve the required balance as  $a \rightarrow 0$ ,  $\alpha_0$  must satisfy  $J_n(\alpha_0 r_s) = 0$ ,  $n \geq 0$ . Balancing higher-order corrections leads to the conclusion that for  $n = 0$  then

$$\alpha = \alpha_{00} + a\alpha_{10} + \dots, \tag{6.1}$$

where  $\alpha_{00}$  and  $\alpha_{10}$  are given by

$$J_0(\alpha_{00} r_s) = 0 \quad \text{and} \quad \alpha_{10} r_s = -\frac{\alpha_{00}^{7/3} \pi Y_0(\alpha_{00} r_s)}{2.002 J_1(\alpha_{00} r_s)}. \tag{6.2}$$

Meanwhile, for  $n > 0$  the appropriate solution is

$$\alpha = \alpha_{0n} + a^{2n} \alpha_{1n} + \dots, \tag{6.3}$$

where  $\alpha_{0n}$  and  $\alpha_{1n}$  satisfy

$$J_n(\alpha_{0n}r_s) = 0 \quad \text{and} \quad \alpha_{1n}r_s = -\frac{\alpha_{0n}^{2n}\pi Y_n(\alpha_{0n}r_s)}{4^n n!(n-1)!J'_n(\alpha_{0n}r_s)}. \quad (6.4)$$

These asymptotic predictions are illustrated in figure 3 and figures 7–9 and they are seen to be in remarkably good agreement with the numerical solutions. Indeed, results (6.1)–(6.4) encapsulate the small-body-radius limit of all the computed modes with the exception of the first mode in the  $n \neq 0$  case for which we have already noted that  $\alpha \rightarrow 0$  as  $a \rightarrow 0$ . When  $n > 0$  this additional solution can be isolated as follows. As  $\alpha r_s \ll 1$ , the eigenrelation (5.2) becomes, at leading order,

$$1.001 \approx \frac{n^2}{a^2 \alpha^{2/3}} \frac{\alpha a}{n} = \frac{n \alpha^{1/3}}{a},$$

so that

$$\alpha \sim (1.001a/n)^3 \quad \text{and} \quad \Omega \sim 2.297 (1.001a/n)^2. \quad (6.5)$$

Note that these leading-order terms are independent of  $r_s$ . In fact, this is the behaviour governing the first neutral solution of (4.8) and also those described by DH2. Thus, as  $r_s \rightarrow \infty$  this structure persists; however as  $a$  increases the solution curve for this first mode quickly reverts to having the behaviour similar to that of the higher modes. This phenomenon is immediately apparent in figure 9 where this behaviour also appears to some extent in the higher modes.

In connection with figure 3 and our numerical solution of the axisymmetric eigenrelation (5.1) we asserted that the kinking feature which appears in the higher modes delimits the small- $a$  solutions found by DH1. That this is the case is easiest to observe if the shockless relation (4.4) is rewritten in the alternative form

$$\frac{\text{Ai}'(\xi_0)}{\int_{\xi_0}^{\infty} \text{Ai}(\xi) d\xi} = i^{1/3} \alpha^{4/3} \frac{Y_0(\alpha a) + iJ_0(\alpha a)}{Y_1(\alpha a) + iJ_1(\alpha a)}. \quad (6.6)$$

Now DH1 showed that as  $a \rightarrow 0$  so solutions of this equation satisfy  $\alpha \rightarrow \infty$ ,  $\alpha a \rightarrow 0$ . Using the well-known small-argument forms

$$J_0(\delta) \sim 1 + O(\delta^2), \quad J_1(\delta) \sim \frac{1}{2}\delta + \dots, \quad Y_0(\delta) \sim \frac{2}{\pi} \ln(\frac{1}{2}\delta) + \dots, \quad Y_1(\delta) \sim -\frac{2}{\pi\delta} + \dots, \quad (6.7)$$

as  $a \rightarrow 0$  the right-hand side of (6.6) tends to  $i^{1/3} \alpha^{4/3} Y_0(\alpha a)/Y_1(\alpha a)$ . Meanwhile, in conjunction with eigenrelation (5.1), we have that in the same limit  $\alpha r_s \rightarrow \infty$  and as  $J_0(\alpha r_s)$  and  $Y_0(\alpha r_s)$ , although oscillatory, are bounded, so the second terms in both the numerator and denominator of the right-hand side become much less than the first ones (assuming  $J_0(\alpha r_s) \neq 0$ ). Consequently, the eigenrelations (5.1) and (6.6) tend to the same form at leading order and hence the small- $a$  solutions of DH1 are approached. Of course, this argument relies on the assumption that  $J_0(\alpha r_s) \neq 0$ : if  $\alpha$  happens to be such that  $\alpha r_s$  is close to a zero of  $J_0$  our analysis requires some modification. This explains why the kinks of figure 3 identify the remnants of the mode of DH1 but do not delimit the whole of their curve as our solutions veer away around points near roots of  $J_0(\alpha r_s) = 0$ .

6.2. Limit as  $a \rightarrow r_s$ .

Investigation of this case reveals that there are two possible asymptotic limits in this situation which corresponds to the case in which the shock position nears the surface of the cone. The first asymptotic structure tackles the case  $\alpha(r_s - a) \ll 1$  in the axisymmetric problem. Then, on expanding the Bessel functions in (5.1) in powers of  $\alpha(r_s - a)$  we find that  $\alpha$  is given by

$$\alpha = (r_s - a)^{-3/7} + \frac{3}{14r_s}(r_s - a)^{4/3} + \dots \tag{6.8}$$

This expression is found to agree extremely well with the first-mode solutions for the axisymmetric problem for all values of  $r_s$ , as illustrated in figures 5 and 6.

When  $\alpha(r_s - a) \sim O(1)$ , assuming  $\alpha r_s \gg 1$  and  $\alpha a \gg 1$  another solution may be obtained for  $\alpha$ . Substituting the expansions of the Bessel functions in (5.1) and (5.2) for large argument gives expressions for  $\alpha$  in each case. For the axisymmetric problem we find that

$$\alpha = \frac{m\pi}{r_s - a} + \frac{(r_s - a)^{1/3}}{(m\pi)^{4/3}} + \dots, \tag{6.9}$$

for  $m = 1, 2, \dots$ . Thus, for  $m = 1$ , this expression corresponds to the second mode and in general the choice  $m = m'$  corresponds to the  $(m' + 1)$ th mode. The agreement is seen to be very close in figures 4–6. For the non-axisymmetric problem, similar analysis reveals that

$$\alpha = \frac{(2m - 1)\pi}{2(r_s - a)} - \frac{n^2(r_s - a)^{-1/3}}{r_s^2((2m - 1)\frac{1}{2}\pi)^{2/3}} + \dots, \tag{6.10}$$

for  $n > 0$  and  $m = 1, 2, \dots$ . Here  $m = 1$  corresponds to the first mode so that (6.10) describes all the modes for  $a$  and  $r_s$  large. The prediction given by (6.10) is shown in figures 7–9 where the agreement is seen to be excellent. At leading order (6.10) gives  $\alpha$  independent of  $n$ ; a feature that can be observed in the computed solutions for  $a \rightarrow r_s$  by, for example, comparing figures 7(a) and 8 or figures 9(a) and 9(b).

**7. Temporal stability**

Although neutral modes are of frequent theoretical concern, from a practical viewpoint it is often worthwhile to examine growth rates of non-neutral disturbances. In this section we consider the temporal evolution of viscous modes and, in §8, shall direct attention to the equivalent spatial problem. Here we solved eigenrelations (4.3) and (4.7) with  $\alpha$  real and  $\Omega$  complex; it is clear that as from the outset we have sought modes proportional to  $\exp[i(\alpha X + n\phi - \Omega\tau)]$  then if  $\Omega = \Omega_r + i\Omega_i$  we have that  $\Omega_i < 0$  corresponds to stability and  $\Omega_i > 0$  instability.

We begin our account of temporal modes by initially focusing on the axisymmetric case  $n = 0$  and figure 10 illustrates the dependence of  $\Omega_i$  on the wavenumber  $\alpha$  for a selection of shock locations  $r_s$  and local cone radii  $a$ . Figure 10(a,b) shows that for prescribed  $r_s$  the growth rates of unstable modes tend to increase with  $\alpha$ . The fairly violent exchanges between regions of stability and instability are reminiscent of the temporal-growth curves given in CH. They proved that these rapid changes are associated with wavenumbers at which  $\Omega_r$  is discontinuous as a function of  $\alpha$  and switches between large positive and negative values. Our calculations reveal that exactly the same phenomenon is at work in this hypersonic-cone flow. Figure 10(a,c,d) shows the effects on temporal growth rates of increasing  $r_s$  whilst maintaining the

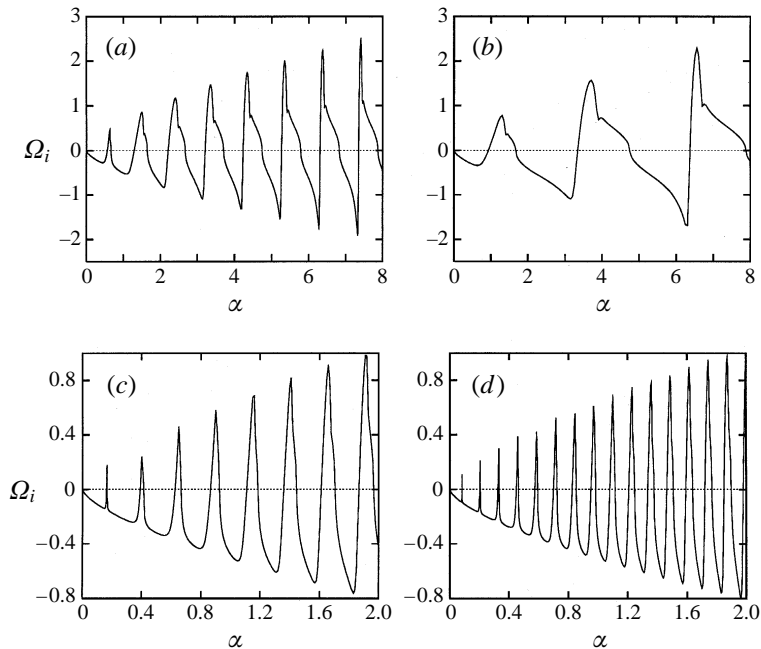


FIGURE 10. The temporal growth rates  $\Omega_i$  for non-neutral axisymmetric modes plotted as functions of the wavenumber  $\alpha$  for a selection of shock positions  $r_s$  and local cone radius  $a$ . In (a–d),  $(r_s, a) = (4, 1), (4, 3), (16, 4)$  and  $(32, 8)$  respectively.

ratio  $a/r_s$  constant. Not surprisingly, as the distance between the shock and the cone surface increases so the effect of the shock lessens and growth rates typically slightly diminish. In addition, it is clear that as  $r_s$  grows so the domains of wavenumber space in which instability persists shrink. Indeed, when  $r_s$  is large, figure 10(d) suggests that the overwhelming majority of wavenumbers are associated with stable waves and it is only quite tiny wavenumber bands which are unstable.

Turning now to non-axisymmetric disturbances, in figure 11 we consider the temporal characteristics of modes of azimuthal wavenumber  $n = 1$ . The two cases shown,  $r_s = 4$  and  $a = 1, 3$ , illustrate some features which are distinct from the corresponding axisymmetric calculations (see figure 10a,b). Although there is no great change in the amplification rates, it is noticeable that the  $n = 1$  modes are unstable over a significantly reduced proportion of wavenumber space. In particular, for  $r_s = 4$  and  $a = 3$ , virtually all the possible modes lie within the stable domain and only a few selected wavenumbers correspond to growing disturbances. These general comments concerning the differences in the temporal rates between axisymmetric and non-axisymmetric disturbances continue to hold for higher values of  $n$ . In figure 12(a,b) we show the respective curves for  $n = 2$ ,  $r_s = 4$  and  $a = 1, 3$ ; in particular the maxima in the growth rates seem insensitive to  $n$ . Modes with  $n = 2$ ,  $r_s = 1$  and  $a = 0.25, 0.75$  are illustrated in figure 12(c,d) and once more we remark as  $r_s$  shrinks so a greater proportion of wavenumber space is associated with growing modes but increases in the cone radius  $a$  have the opposite effect.

One final comparison between figures 10, 11 and 12 which deserves comment is the form of the unstable wavenumber bands as  $\alpha$  increases. Non-axisymmetric disturbances tend to exhibit shrinking of these intervals (see figures 11a or 12d for

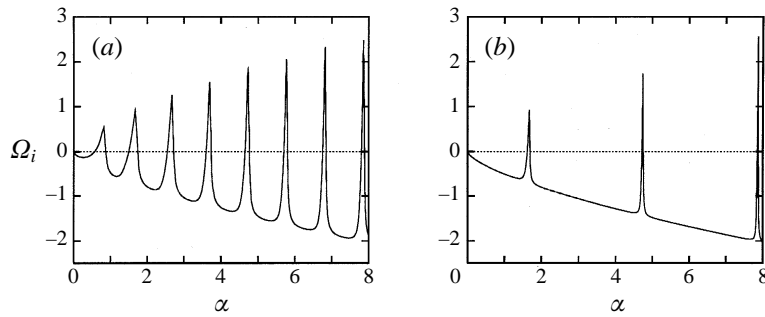


FIGURE 11. Temporal growth rates  $\Omega_i(\alpha)$  for  $n = 1$  non-axisymmetric modes with (a)  $(r_s, a) = (4, 1)$  and (b)  $(r_s, a) = (4, 3)$ .

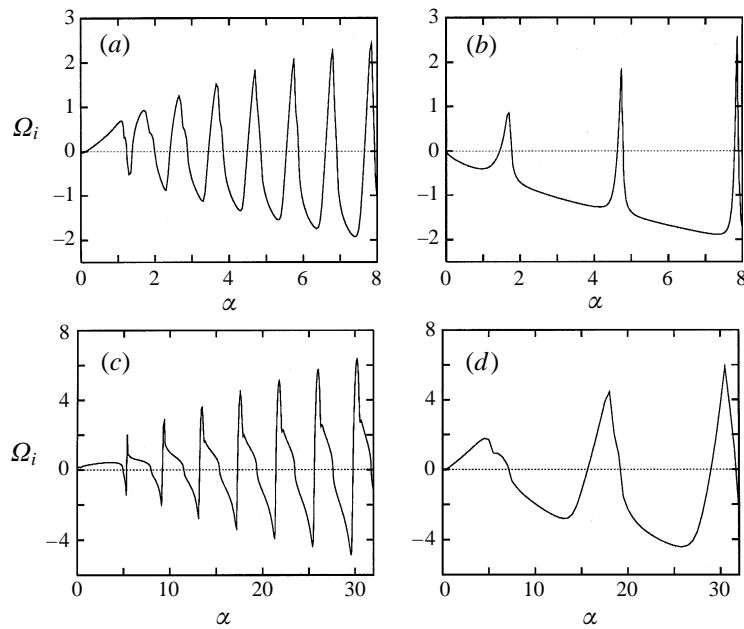


FIGURE 12. Temporal growth rates  $\Omega_i(\alpha)$  for  $n = 2$  modes and, in (a-d),  $(r_s, a) = (4, 1), (4, 3), (1, 0.25)$  and  $(1, 0.75)$  respectively.

example) but axisymmetric modes tend to show the opposite trend (a feature best observed in figure 10d).

### 8. Spatial stability computations

We now concern ourselves with an examination of the spatial evolution of disturbances so that we concentrate on solutions of (4.3) and (4.7) with  $\Omega$  real and  $\alpha$  complex. The reader is reminded that with  $\alpha = \alpha_r + i\alpha_i$  then  $\alpha_i > 0$  is indicative of stability while  $\alpha_i < 0$  denotes spatial instability.

Let us commence our discussion with the axisymmetric modes. Figure 13 shows the dependence of the spatial growth-rate parameter  $\alpha_i$  on the mode frequency  $\Omega$  for a variety of shock positions  $r_s$  and cone radii  $a = r_s/4$  and  $3r_s/4$ . For each pair  $(r_s, a)$  there is a complete family of modes, as we saw in our account of neutral disturbances,

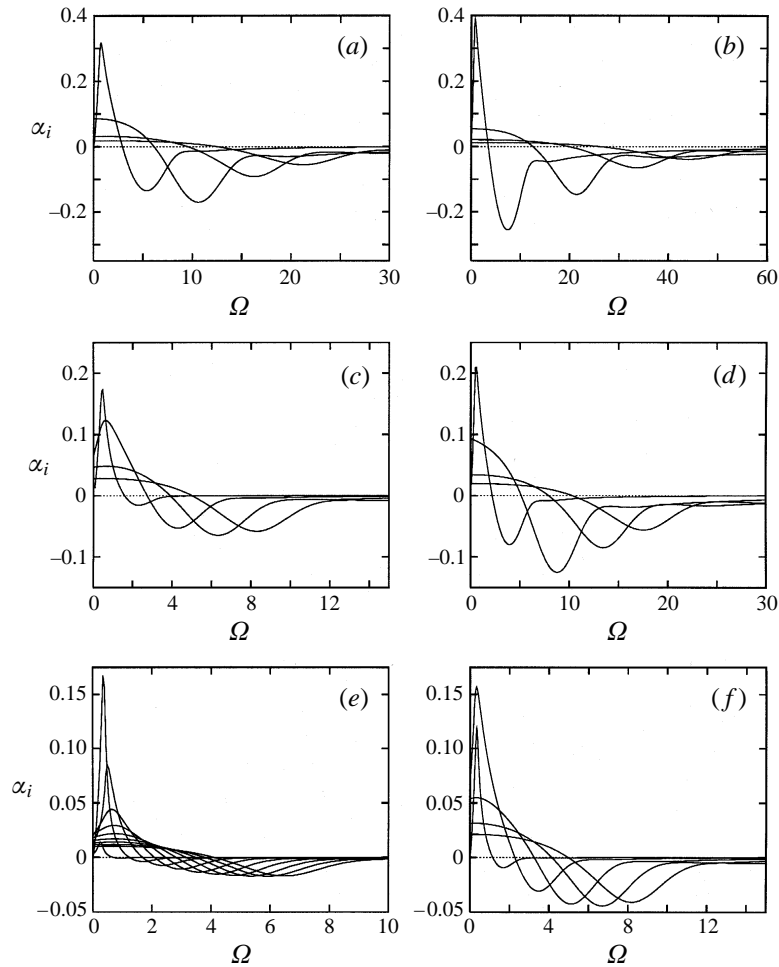


FIGURE 13. Spatial growth-rate parameters  $\alpha_i(\Omega)$  for non-neutral axisymmetric modes. In (a–f) we show the growth rates for the first few modes relating to the parameter choices  $(r_s, a) = (1, 0.25)$ ,  $(1, 0.75)$ ,  $(4, 1)$ ,  $(4, 3)$ ,  $(16, 4)$  and  $(16, 12)$  respectively.

and it is clear that for each member of the family there is a cut-off frequency  $\Omega_c$  such that for  $\Omega < \Omega_c$  that particular mode is stable but it becomes unstable if  $\Omega > \Omega_c$ . However, we also observe that the growth rate rapidly approaches zero at high frequencies. Figure 13(a) shows the first four modes when  $r_s = 1$ ,  $a = 0.25$  and we immediately see that the most unstable of the modes is not the first one, as might have been anticipated, but instead is the second. As  $a$  increases, see figure 13(b), the first mode takes over as the most unstable one and we notice that the spatial growth rates tend to increase. For larger  $r_s$  and smallish cone radius  $a$ , see figure 13(c), it is now the third mode which appears to be the most important but again, as the shock moves further from the surface of the cone, it is hardly surprising that the computed growth rates tend to fall. These trends can be summed up by: (i) amplification rates grow as  $a \rightarrow r_s$ ; (ii) they diminish as  $r_s$  grows and (iii) the index of the most unstable mode rises with  $r_s$  but falls with  $a$ . Further verification of these assertions is provided by figure 13(d–f).

Figure 14 summarizes the spatial amplification rates for the same choices of  $(r_s, a)$

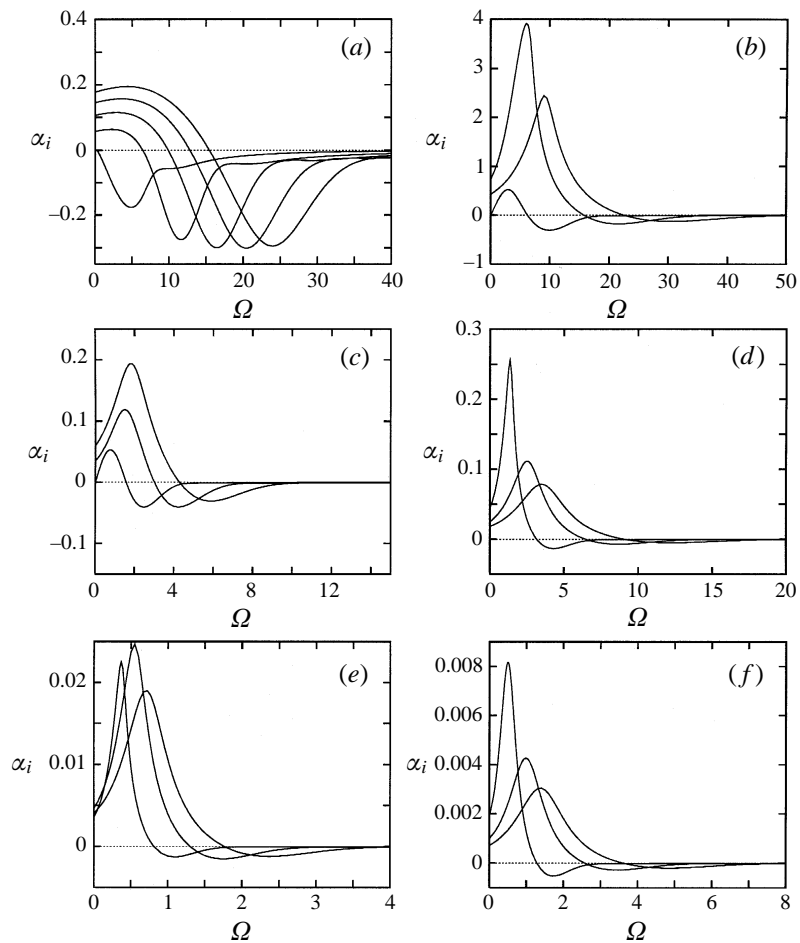


FIGURE 14. Spatial growth-rate parameters  $\alpha_i(\Omega)$  for non-neutral non-axisymmetric modes with azimuthal wavenumber  $n = 1$ . In (a–f) the choices for  $r_s$  and  $a$  are as given in figure 13.

as considered in figure 13, but with the important difference that the modes are non-axisymmetric with azimuthal wavenumber  $n = 1$ . On contrasting figures 13(a) and 14(a) it is striking how the most unstable mode in the non-axisymmetric case is the fourth one compared with the second one in the axisymmetric problem. Furthermore, when  $n = 1$  it appears that the overall spatial growth rates are enhanced and that the difference in growth rates of adjacent modes is really quite small. If  $a$  is now increased, see figure 14(b), the contrasts between the  $n = 0$  and  $n = 1$  solutions largely disappear. In both cases, it is now the first mode which is the most unstable and the corresponding growth rates are very similar indeed. The enhanced growth rates for the  $n = 1$  modes over their  $n = 0$  counterparts for smallish  $r_s$  is reversed once  $r_s$  is increased. Figure 14(c,d) shows  $n = 1$  modes associated with  $r_s = 4$ ,  $a = 1$  and 3, cf. figure 13(c,d). At the smaller value of  $a$  the amplification rates of the axisymmetric modes are slightly the greater but by the time  $a = 3$  the difference is very much more marked. This trend is continued in figure 14(e,f) and we observe that for  $r_s = 16$ ,  $a = 12$  the growth rates of the axisymmetric modes can be up to fifty times those relating to the  $n = 1$  disturbances.

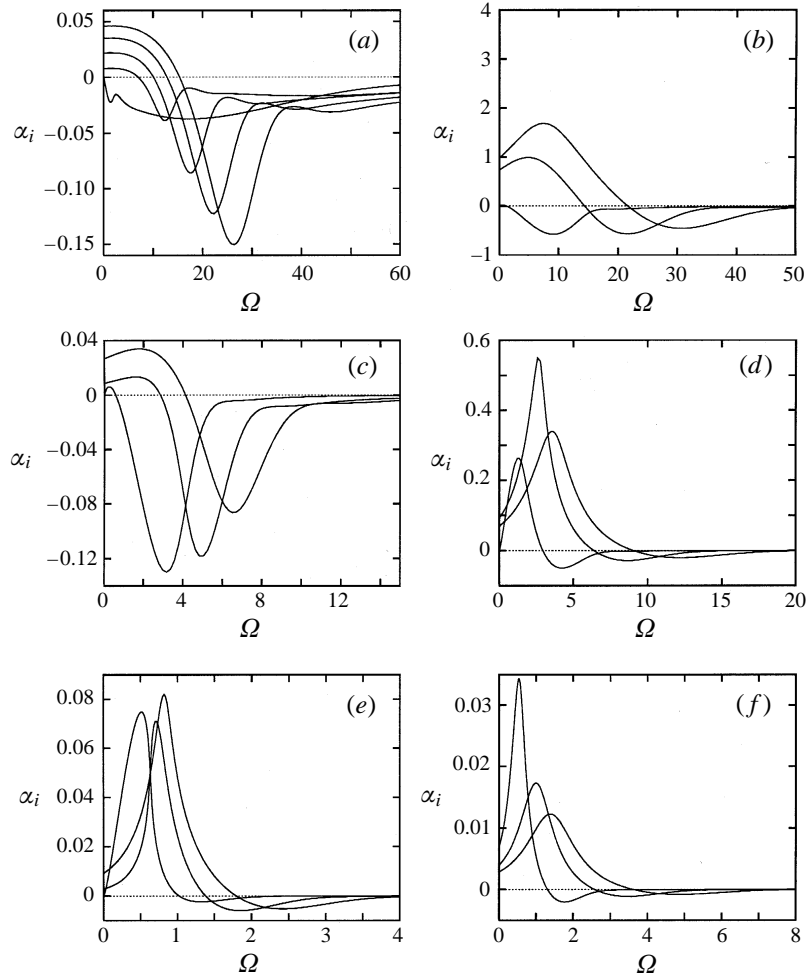


FIGURE 15. Spatial growth-rate parameters  $\alpha_i(\Omega)$  for non-neutral non-axisymmetric modes with azimuthal wavenumber  $n = 2$ . In (a–f) the choices for  $r_s$  and  $a$  are as given in figure 13.

Figure 15 presents the results of a few calculations aimed at investigating the role played by larger azimuthal wavenumbers  $n$ . Comparing figure 15(a,b) with figure 14(a,b) we conclude, at least when  $r_s = 1$ , that modes with  $n = 1$  are potentially more dangerous than their  $n = 2$  counterparts when the cone radius is reasonably small. However, as  $a$  increases, so the relative importances of the  $n = 1$  and  $n = 2$  modes is exchanged; see figures 14(b) and 15(b) pertaining to  $a = 0.75$ . When the shock moves further from the cone, it appears that  $n = 2$  modes always have larger amplification rates than the  $n = 1$  disturbances; cf. figures 14(c,d) and 15(c,d). Indeed, for all the values of  $a$  tested with  $r_s = 16$  we found that  $n = 2$  modes typically have enhanced growth rates when compared to the corresponding  $n = 1$  results; cf. figures 14(e,f) and 15(e,f).

We conclude this brief account of spatially unstable modes by examining the dependences of the maximum spatial growth rates as functions of cone radius  $a$  for various azimuthal wavenumbers  $n$ . Figure 16 shows the forms of the  $n = 0, 1, 2$  amplification factors for shock positions  $r_s = 1, 4$  and 16 respectively. First, it should



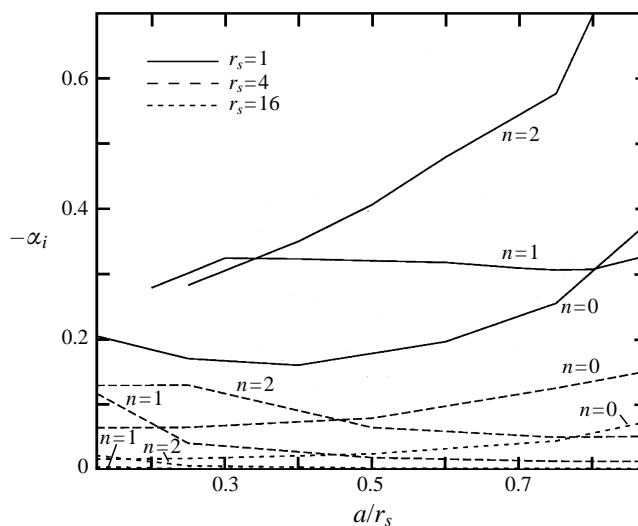


FIGURE 16. Maximum spatial growth-rate parameters  $-\alpha_i$  as functions of the local cone radius  $a/r_s$  for shock positions  $r_s = 1, 4, 16$ . Shown in each case are the results for the  $n = 0, 1, 2$  modes.

be remarked that the slight crudeness of the figure is entirely a consequence of the difficulty of the computation. For each selected set of  $r_s$ ,  $a$  and  $n$  it was necessary to calculate a whole family of modes as functions of  $\Omega$ , of the type shown in any of figures 13–15, and then identify the most unstable of these. This lengthy calculation yields just one point on one line in figure 16 and resource constraints made calculation of numerous points on each line infeasible. That having been said though, there is enough information for us to draw some general conclusions. It appears that the behaviour of the axisymmetric modes is largely independent of  $r_s$  in as much that maximal spatial amplification rates grow with  $a$ . Unsurprisingly, overall growth rates reduce as the shock moves away from the cone ( $r_s \rightarrow \infty$ ).

The influence of the shock appears to be much more dramatic for the non-axisymmetric disturbances. Figure 16 proves that for a shock well away from the cone the  $n \neq 0$  modes have very small growth rates and that it is the axisymmetric mode that may be expected to dominate the flow characteristics, at least for a wide range of cone radii. As  $a \rightarrow r_s$ , so that the shock nears the cone surface, growth rates tend to rise but, at least when  $r_s = 16$ , the axisymmetric mode seems to retain its prominence. Figure 16 suggests that for lesser  $r_s$  it is not the axisymmetric mode which is the most important and the closeness of the shock to the cone has a significant effect on the non-axisymmetric disturbances. From the results presented in figure 16 for non-axisymmetric modes it appears that there is no general trend of how the maximum amplification behaves as  $a$  increases. For the choice  $r_s = 1$ , it appears that the  $n = 2$  modes have the largest growth rates. It is eminently plausible that as  $r_s$  shrinks so the azimuthal wavenumber of the most strongly amplified mode grows. However, in assessing the relative importance of the various modes for any particular flow it has to be remembered that the viscous disturbances examined here are most likely to be triggered by roughness on the surface of the cone. The exact form of this roughness and, in particular, its azimuthal distribution, is likely to preferentially excite certain modes. Thus although it is certainly useful to know the form of the maximum spatial growth rates of each mode as functions of cone radius, it is less certain whether comparison of growth rates for different  $n$  is of particular relevance.

Nevertheless, we can briefly summarize our findings with the comments that for axisymmetric modes the maximal growth rates increase with cone radius for fixed  $r_s$  and that whilst axisymmetric modes appear to be the most dangerous when the shock is located in the outer reaches of the boundary layer, as  $r_s$  reduces so the azimuthally dependent modes assume an increasing prominence.

## 9. Discussion

In this study we have conducted a linear stability analysis of viscous modes in flow past a slender cone. The solutions obtained have demonstrated that the effect of the shock within the flow is significant and that the modes which could exist in the absence of the shock are now almost totally destroyed. The influence of the shock is always there, even in the limit  $r_s \rightarrow \infty$ , unlike the planar case (see CH), and gives rise to multiple modes; an explanation for this is related to the fact that the shock allows incoming as well as outgoing waves.

We can now show that new viscous modes are indeed introduced even as  $r_s \rightarrow \infty$  by returning to the axisymmetric dispersion relation (5.1). If  $r_s$  is large, we scale  $\alpha = \bar{\alpha}/r_s$ ,  $a = \bar{a}r_s$ ,  $\Omega = r_s^{-2/3}\bar{\Omega}$  so that we have

$$\frac{i^{-1/3}\text{Ai}'(\bar{\xi}_0)}{\int_{\bar{\xi}_0}^{\infty}\text{Ai}(\xi)d\xi} = \bar{\alpha}^{4/3}r_s^{-4/3}\frac{J_0(\bar{\alpha})Y_0(\bar{\alpha}\bar{a}) - J_0(\bar{\alpha}\bar{a})Y_0(\bar{\alpha})}{J_0(\bar{\alpha})Y_1(\bar{\alpha}\bar{a}) - J_1(\bar{\alpha}\bar{a})Y_0(\bar{\alpha})}, \quad (9.1)$$

where  $\bar{\xi}_0 = -i^{1/3}\bar{\Omega}\bar{\alpha}^{-2/3}$ . For neutral modes we have the usual result  $\bar{\xi}_0 \approx 2.297i^{1/3}$  and so for both sides of (9.1) to be  $O(1)$  the denominator of the right-hand side must vanish at leading order. Since Bessel functions oscillate as their (real) arguments  $\rightarrow \infty$ , there is guaranteed to be a infinite family of solutions of

$$J_0(\bar{\alpha})Y_1(\bar{\alpha}\bar{a}) - J_1(\bar{\alpha}\bar{a})Y_0(\bar{\alpha}) = 0.$$

For example, if  $\bar{a} = \frac{1}{2}$ , then  $\bar{\alpha} = \bar{\alpha}_n = 3.59, 9.60, 15.82, \dots$  If we write  $\bar{\alpha} = \bar{\alpha}_n + r_s^{-4/3}\hat{\alpha}$  then we can take Taylor expansions of the right-hand side of (9.1) to deduce  $\hat{\alpha}$ . It is clear that we have found multiple solutions of (9.1) as  $r_s \rightarrow \infty$  which correspond to neutral waves. We can then safely conclude that there are non-neutral solutions of our dispersion relation in the same limit and similar, though slightly more complicated, arguments hold for the non-axisymmetric problem. We re-emphasize that these multiple solutions are induced by the shock for in its absence this situation cannot arise.

In reviewing the results of our investigations we highlight some of the more significant findings. The neutral curves generated in §5 are in good agreement with the asymptotic solutions discussed in §6 valid in the limits of small cone radius or  $a \rightarrow r_s$ . Of interest is the observation that over much of the range  $0 < a < r_s$  the calculated curves are remarkably well approximated by one or other of the simple asymptotic forms. The non-neutral computations verify the expectation that the overall spatial growth rates diminish as the shock moves away from the cone. What may have been less predictable is that for large values of  $r_s$  the maximal spatial growth rates are usually associated with the axisymmetric modes and the non-axisymmetric disturbances experience far weaker amplification. For shocks nearer the surface of the cone the situation is more complicated and the two types of mode have similar growth rates – which particular mode is then the fastest growing is dependent on the exact values of  $a$  and  $r_s$ .

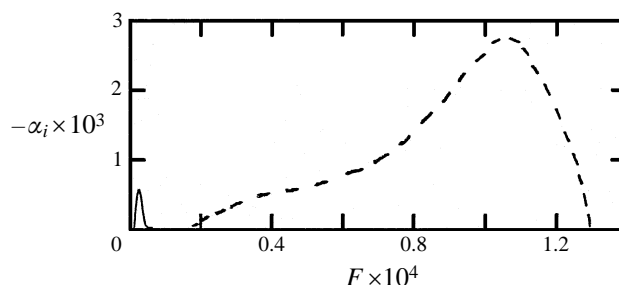


FIGURE 17. Scaled amplification rate  $-\alpha_i \times 10^3$  versus non-dimensional frequency  $F \times 10^4$  for  $r_s = 1$ ,  $a = 0.9$  and  $n = 2$ . Dashed line corresponds to experimental results of Stetson *et al.* (1983).

In view of advances in the aircraft and space industries, there appear to have been few modern experiments directed towards investigating the stability of hypersonic flows over axisymmetric bodies in general, and cones in particular. However some numerical attacks on this problem appear to support many of our findings. Tai & Kao (1994) report agreement between their Navier–Stokes solver and experiments on high-speed flow past slender cones. Computations by Stilla (1994) and Leung & Emanuel (1995) have also modelled this flow at  $M_\infty = 8$ . Their work shows that the stability of the flow is sensitive to the viscous–inviscid interaction zone within the boundary layer and that proper resolution of the shock layer is crucial. Interestingly, Stilla (1994) found that the use of different viscosity laws had a far less dramatic effect on the results than might have been anticipated. (We noted earlier that our analysis here is unaffected by choice of viscosity law.) Calculations by Malik & Spall (1991) showed that in flow over axisymmetric bodies the transverse curvature involved is a vital term in the stability equations; they remarked that there are significant discrepancies between sharp-cone experiments and planar stability theory. They also raised the possibility that non-parallelism might play some role in the stability of the flow. This aspect has been reinforced by the linear stability analysis of Stuckert & Reed (1994) for very high-speed flows at Mach 25. They included chemical reaction terms in their formulation and used parabolized stability equations combined with a shock fitting technique to investigate inviscid instabilities. In order to achieve any agreement with experimental results, Stuckert & Reed (1994) noted that inclusion of non-parallelism was essential.

An attempt was made to compare the current results with the growth rates measured by Stetson *et al.* (1983). This was achieved by taking the values of the Mach number and (dimensional) temperature just behind the shock to be the corresponding boundary-layer edge values of the experiments. The shock is not mentioned in the description of the experiments. These quantities are required to calculate the length and time scales of (3.1). The boundary-layer skin friction  $\lambda$  was taken to be 0.332 (the value for Chapman’s viscosity law) and the viscosity at the wall was evaluated by using Sutherland’s law. The results of Stetson *et al.* (1983) for amplification rates  $-\alpha_i \times 10^3$  versus non-dimensional frequency  $F \times 10^4$  are shown by the dashed curve in figure 17 for  $M = 6.8$  and  $Re = 2.99 \times 10^6$  with a wall temperature of  $1155^\circ\text{R}$  for a  $7^\circ$  half-angle cone (taken from figure 19 in their paper). Also shown are the (appropriately scaled) results for  $r_s = 1$ ,  $a = 0.9$  and  $n = 2$  for the mode which gives the maximum growth rate. It can be seen that the current disturbances occur for much lower frequencies than those observed experimentally and have smaller amplification rates. Thus, it appears that the shock has a dramatic effect on the instability of this

flow. However, it must be recalled that our analysis has concentrated on viscous instability modes which are amenable to triple-deck description. One possible resolution of the relatively poor agreement between our theoretical results and the experimental findings is that Stetson *et al.* (1983) did not observe the viscous disturbances but some other, possibly more rapidly growing, mode type. There is the obvious need to establish more information about the stability of axisymmetric hypersonic boundary-layer flows before more reliable comparison of theory and experiment can be made.

In this work we have investigated parameter regimes in which non-parallelism is negligible compared with the roles played by the shock and curvature. To extend our study it would seem that inclusion of non-parallel effects would be desirable although we note that this is yet to be done for the simpler problem of hypersonic flow past a plane wedge. An asymptotic analysis of the inviscid stability of an axisymmetric hypersonic flow would also be of interest. Extension of the present analysis into nonlinear regimes would provide a challenging problem although we mention that the framework laid here provides the starting point for a weakly nonlinear analysis; this theory for the wedge flow may be found in Seddougui & Bassom (1994).

We are indebted to the referees whose comments led to substantial improvements to this article. Special thanks are due to the referee who encouraged us to undertake the non-neutral work described in §§7,8.

Discussions with Professor P. Hall, Dr S. J. Cowley and Dr P. W. Duck are gratefully acknowledged. We thank Dr S. R. Otto for assistance in generating figure 1.

This article was completed and revised whilst the authors were on separate study visits at the School of Mathematics, University of New South Wales, Sydney. We are grateful to Dr P. J. Blennerhassett and the School of Mathematics for their hospitality. Our visits were supported by the Australian Research Council; A.P.B. acknowledges additional support from the Royal Society of London.

#### REFERENCES

- ABRAMOWITZ, M. & STEGUN, I. A. 1964 *A Handbook of Mathematical Functions*. Frankfurt: National Bureau of Standards.
- BALAKUMAR, P. & REED, H. L. 1991 Stability of three-dimensional supersonic boundary layers. *Phys. Fluids A* **3**, 617–632.
- BLACKABY, N. D., COWLEY, S. J. & HALL, P. 1993 On the instability of hypersonic flow past a flat plate. *J. Fluid Mech.* **247**, 369–416.
- BROWN, S. N., CHENG, H. K. & LEE, C. J. 1990 Inviscid viscous interaction on triple-deck scales in a hypersonic flow with strong wall cooling. *J. Fluid Mech.* **220**, 309–337.
- CHANG, C.-L., MALIK, M. R. & HUSSAINI, M. Y. 1990 Effects of shock on the stability of hypersonic boundary layers. *AIAA Paper* 90-1448.
- COWLEY, S. J. & HALL, P. 1990 On the instability of the hypersonic flow past a wedge. *J. Fluid Mech.* **214**, 17–42 (referred to herein as CH).
- DANDO, A. H. & SEDDOUGUI, S. O. 1993 The compressible Görtler problem in two-dimensional boundary layers. *IMA J. Appl. Maths* **51**, 27–67.
- DUCK, P. W. 1984 The effect of a surface discontinuity on an axisymmetric boundary layer. *Q. J. Mech. Appl. Maths* **37**, 57–74.
- DUCK, P. W. 1990 The inviscid axisymmetric stability of the supersonic flow along a circular cylinder. *J. Fluid Mech.* **214**, 611–637.
- DUCK, P. W. & HALL, P. 1989 On the interaction of Tollmien–Schlichting waves in axisymmetric supersonic flows. *Q. J. Mech. Appl. Maths* **42**, 115–130 (referred to herein as DH1).
- DUCK, P. W. & HALL, P. 1990 Non-axisymmetric viscous lower-branch modes in axisymmetric supersonic flows. *J. Fluid Mech.* **213**, 191–201 (referred to herein as DH2).

- DUCK, P. W., LASSEIGNE, D. G. & HUSSAINI, M. Y. 1995 On the interaction between the shock-wave attached to a wedge and freestream disturbances. *Theor. Comput. Fluid Dyn.* **7**, 119–139.
- DUCK, P. W. & SHAW, S. J. 1990 The inviscid stability of supersonic flow past a sharp cone. *Theor. Comput. Fluid Dyn.* **2**, 139–163.
- FISCHER, M. C. & WEINSTEIN, L. M. 1972 Cone transitional boundary-layer structure at  $M_e = 14$ . *AIAA J.* **10**, 699–701.
- GRUBIN, S. E. & TRIGUB, V. N. 1993 The long-wave limit in the asymptotic theory of hypersonic boundary-layer stability. *J. Fluid Mech.* **246**, 381–395.
- HAYES, W. D. & PROBSTEIN, R. F. 1966 *Hypersonic Flow Theory*. Academic.
- KERIMBEKOV, R. M., RUBAN, A. I. & WALKER, J. D. A. 1994 Hypersonic boundary-layer separation on a cold wall. *J. Fluid Mech.* **274**, 163–195.
- LEUNG, K. K. & EMANUEL, G. 1995 Hypersonic inviscid and viscous flow over a wedge and cone. *J. Aircraft* **32**, 385–391.
- MALIK, M. R. & SPALL, R. E. 1991 On the stability of compressible flow past axisymmetric bodies. *J. Fluid Mech.* **228**, 443–463.
- PRUETT, C. D. & CHANG, C.-L. 1995 Spatial direct numerical simulation of high-speed boundary-layer flows—Part II: Transition on a cone in Mach 8 flow. *Theor. Comput. Fluid Dyn.* **7**, 397–424.
- SEDDOUGUI, S. O. 1994 Stability of hypersonic flow over a cone. In *Transition, Turbulence and Combustion* (ed. M. Y. Hussaini, T. B. Gatski & T. L. Jackson), pp. 50–59. Kluwer.
- SEDDOUGUI, S. O. & BASSOM, A. P. 1994 Nonlinear instability of hypersonic flow past a wedge. *Q. J. Mech. Appl. Maths* **47**, 557–582.
- SEDDOUGUI, S. O., BOWLES, R. I. & SMITH, F. T. 1991 Surface-cooling effects on compressible boundary-layer instability, and on upstream influence. *Eur. J. Mech. B/Fluids* **10**, 117–145.
- SMITH, F. T. 1989 On the first-mode instability in subsonic, supersonic or hypersonic boundary layers. *J. Fluid Mech.* **198**, 127–153.
- SMITH, F. T. & BROWN, S. N. 1990 The inviscid instability of a Blasius boundary-layer at large values of the Mach number. *J. Fluid Mech.* **219**, 499–518.
- STETSON, K. F., THOMPSON, E. R., DONALDSON, J. C. & SILER, L. G. 1983 Laminar boundary-layer stability experiments on a cone at Mach 8. Part 1: Sharp cone. *AIAA Paper* 83-1761.
- STEWARTSON, K. 1964 *The Theory of Laminar Boundary Layers in Compressible Fluids*. Oxford University Press.
- STILLA, J. 1994 Engineering transition prediction for a hypersonic axisymmetrical boundary-layer. *J. Aircraft* **31**, 1358–1364.
- STUCKERT, G. & REED, H. L. 1994 Linear disturbances in hypersonic, chemically reacting shock layers. *AIAA J.* **32**, 1384–1393.
- TAI, C. S. & KAO, A. F. 1994 Navier–Stokes solver for hypersonic flow over a slender cone. *J. Spacecr. and Rockets* **31**, 215–222.